Neuron

Article

The Parabrachial Nucleus Directly Channels Spinal Nociceptive Signals to the Intralaminar Thalamic Nuclei, but Not the Amygdala

Graphical Abstract

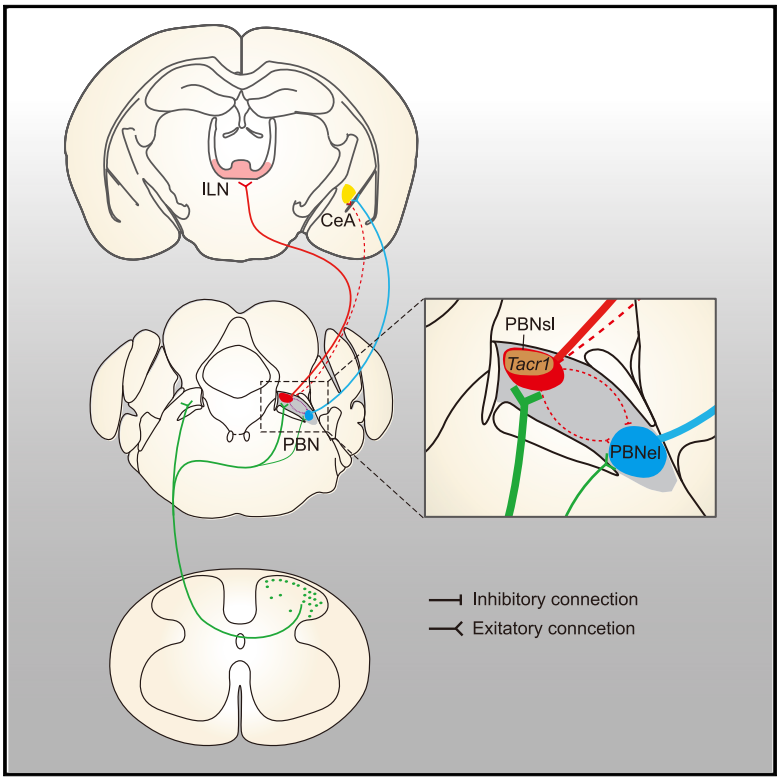

Highlights

- The ipsi- and contralateral spinoparabrachial pathways are functionally distinct
- The ipsilateral spinoparabrachial pathway mediates nocifensive behavior
- *Tacr1*$^{+}$ neurons in the PBN represent the major target of spinal projection
- The PBN relays nociceptive information to the ILN via glutamatergic synapses

Authors

Juan Deng, Hua Zhou, Jun-Kai Lin, ..., Yi-Chao Wei, Xiao-Hong Xu, Yan-Gang Sun

Correspondence

jdeng@ion.ac.cn (J.D.), yangang.sun@ion.ac.cn (Y.-G.S.)

In Brief

Deng et al. demonstrate that the ipsilateral spinoparabrachial pathway mediates nocifensive behavior and identify that the *Tacr1*$^{+}$ neurons in the parabrachial nucleus represent the major target of the spinal projection. The authors also reveal the major downstream pathway for processing nociceptive information.

Deng et al., 2020, Neuron *107*, 909–923
September 9, 2020
https://doi.org/10.1016/j.neuron.2020.06.017

CellPress

Neuron

CellPress

Article

The Parabrachial Nucleus Directly Channels Spinal Nociceptive Signals to the Intralaminar Thalamic Nuclei, but Not the Amygdala

Juan Deng,[1,*] Hua Zhou,[1] Jun-Kai Lin,[1,2] Zi-Xuan Shen,[3] Wen-Zhen Chen,[1,2] Lin-Han Wang,[1,2] Qing Li,[1] Di Mu,[1] Yi-Chao Wei,[1] Xiao-Hong Xu,[1] and Yan-Gang Sun[1,4,5,*]

[1]Institute of Neuroscience, State Key Laboratory of Neuroscience, Center for Excellence in Brain Science & Intelligence Technology, Chinese Academy of Sciences, 320 Yue-Yang Road, Shanghai 200031, China

[2]University of Chinese Academy of Sciences, 19A Yu-quan Road, Beijing 100049, China

[3]Department of Biotechnology, East China University of Science and Technology, 130 Mei-long Road, Shanghai 200237, China

[4]Shanghai Center for Brain Science and Brain-Inspired Intelligence Technology, Shanghai 201210, China

[5]Lead Contact

*Correspondence: jdeng@ion.ac.cn (J.D.), yangang.sun@ion.ac.cn (Y.-G.S.)

https://doi.org/10.1016/j.neuron.2020.06.017

SUMMARY

The parabrachial nucleus (PBN) is one of the major targets of spinal projection neurons and plays important roles in pain. However, the architecture of the spinoparabrachial pathway underlying its functional role in nociceptive information processing remains elusive. Here, we report that the PBN directly relays nociceptive signals from the spinal cord to the intralaminar thalamic nuclei (ILN). We demonstrate that the spinal cord connects with the PBN in a bilateral manner and that the ipsilateral spinoparabrachial pathway is critical for nocifensive behavior. We identify *Tacr1*-expressing neurons as the major neuronal subtype in the PBN that receives direct spinal input and show that these neurons are critical for processing nociceptive information. Furthermore, PBN neurons receiving spinal input form functional monosynaptic excitatory connections with neurons in the ILN, but not the amygdala. Together, our results delineate the neural circuit underlying nocifensive behavior, providing crucial insight into the circuit mechanism underlying nociceptive information processing.

INTRODUCTION

The spinal cord sends information to the brain via multiple ascending pathways (Huang et al., 2019; Hylden et al., 1989; Li and Li, 2000; Liu et al., 2009; Polgár et al., 2010; Spike et al., 2003). These ascending pathways are responsible for processing diverse modalities of somatosensory information, including pain (Duan et al., 2018; Todd, 2010). One of major targets of spinal projection neurons in the brain is the parabrachial nucleus (PBN). It has been shown in rodents that 95% of lamina I projection neurons in the spinal cord project to the PBN (Todd, 2010). The spinoparabrachial pathway has been implicated in the processing of nociceptive information (Bernard et al., 1996; Bester et al., 2000; Jansen and Giesler, 2015; Williams and Ivanusic, 2008). Its functional role in pain is further supported by a recent study indicating that excitatory input to the PBN from the spinal cord is critical for affective component of pain (Huang et al., 2019). Interestingly, in contrast to many other ascending pathways, the spinal cord sends projections to the bilateral PBN (Hylden et al., 1989; Li and Li, 2000; Liu et al., 2009; Spike et al., 2003), raising the question of how the ipsilateral and contralateral spinoparabrachial pathways are involved in nociceptive information processing.

Different physiological processes involve distinct subtypes of neurons in the PBN (Chiang et al., 2019; Maeda et al., 2009; Palmiter, 2018), which form a general alarm system that helps to maintain homeostasis (Palmiter, 2018), with pain being one of the most important. The functional role of the PBN in processing nociceptive information has been demonstrated in both electrophysiological and behavioral studies (Barik et al., 2018; Bourgeais et al., 2001; Chiang et al., 2020). Several neuronal subtypes in the PBN are important for processing and modulating nociceptive information. It has been shown that the activity of calcitonin-gene-related peptide (*CGRP*)-positive neurons in the PBN increased in response to noxious stimuli (Campos et al., 2018). In addition, tachykinin 1 (*Tac1*)-positive neurons in the PBN were found to modulate nocifensive behaviors via the descending pathway (Barik et al., 2018; Roeder et al., 2016). A recent study showed that dynorphin (*Pdyn*)-positive neurons in the PBN may convey nociceptive signals from the spinal cord to the external lateral PBN (PBNel) via a local circuit (Chiang et al., 2020). However, which neuronal subtype in the PBN is targeted by spinal

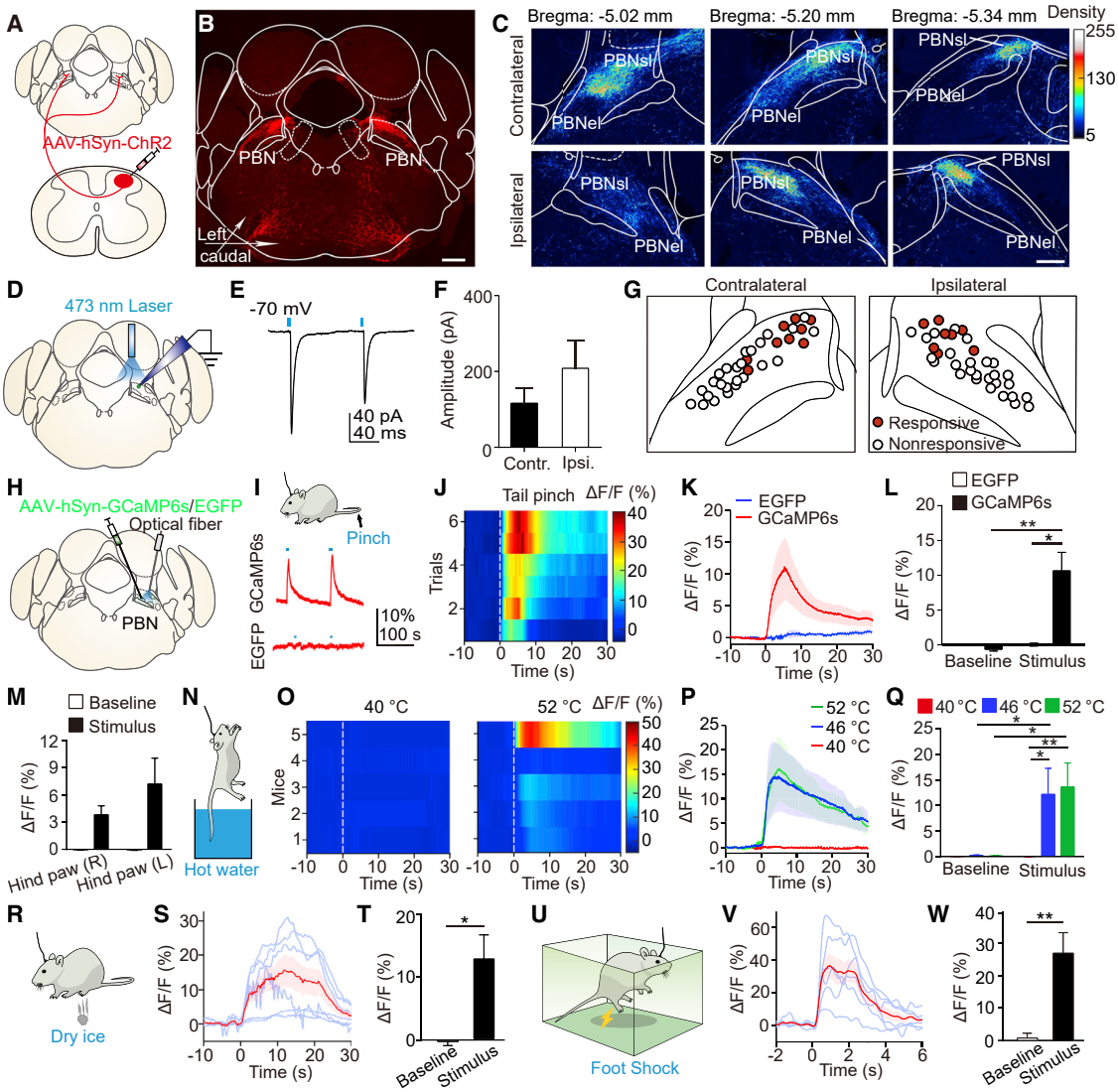

Figure 1. Functional Connectivity Pattern of the Spinoparabrachial Pathway

(A) Schematic for viral injection.

(B) Distribution pattern of spinoparabrachial fibers labeled with mCherry (red) in the PBN. Scale bar, 500 μm.

(C) Average distribution pattern of spinal axon terminals in the PBN (n = 3 mice). Scale bar, 200 μm.

(D) Schematic for slice recording of PBN neurons.

(E) EPSCs recorded in a PBN neuron by light stimulation (473 nm, 1 ms).

(F) Amplitude of light-evoked EPSCs recorded in PBN neurons (n = 8–9 neurons, unpaired Student's t test, p = 0.27).

(G) Location of recorded neurons in the PBN (n = 69 neurons from four mice). Solid symbols, responsive; open symbols, nonresponsive.

(H) Schematic for fiber photometry recording.

(I) Top: schematic showing recording of PBN neurons in response to tail pinch stimulation. Bottom: raw traces of fluorescent signal following pinch stimulation. Blue bars indicate pinch stimulation (5 s).

(J) Heatmap showing the response of PBN neurons to tail pinch stimulation.

(K) Average fluorescent signal in response to tail pinch stimulation (n = 3–5 mice).

(L) Summary of average fluorescent calcium signal changes in PBN neurons evoked by tail pinch stimulation (n = 3–11 mice, two-way ANOVA).

(M) Summary of average fluorescent calcium signal changes in PBN neurons evoked by pinch stimulation (n = 5 mice, paired Student's t test).

(N) Schematic showing recording of PBN neurons in response to thermal stimulation (tail immersion).

(O) Heatmap showing the calcium response of PBN neurons to thermal stimulation.

(P) Average fluorescent signal of GCaMP6s expressed in PBN neurons evoked by thermal stimulation (n = 5 mice).

(Q) Summary of fluorescent signal of GCaMP6s expressed in PBN neurons evoked by thermal stimulation (n = 5 mice, two-way ANOVA).

(R) Schematic showing recording of PBN neurons in response to noxious cold stimulation.

(legend continued on next page)

projection and how these neurons are involved in the processing of nociceptive information remain unknown.

The PBN sends direct projections to multiple targets, including the central nucleus of the amygdala (CeA), intralaminar thalamic nucleus (ILN), ventral tegmental area, and hypothalamus (Chiang et al., 2019; Krout and Loewy, 2000). Diverse outputs of the lateral PBN are involved in distinct components of the nocifensive response (Chiang et al., 2020). The CeA is one of the major targets of the PBN, and it has been proposed that the projection from the PBN to the CeA is critical for the affective component of pain (Missig et al., 2017; Veinante et al., 2013), which is supported by a behavioral study (Han et al., 2015). The ILN represents another major downstream target of the PBN and is also involved in pain processing (Harte et al., 2004; Munn et al., 2009; Thoden et al., 1979). Spontaneous hyperactivity of ILN neurons was detected in patients with deafferentation pain (Rinaldi et al., 1991). Consistently, PBN neurons that send projections to the ILN were shown to be activated by noxious stimuli (Bourgeais et al., 2001). However, the direct downstream target to which the PBN conveys nociceptive information from the spinal cord remains largely unknown.

In this study, we determined the anatomical and functional connections of the spinoparabrachial pathway and examined differential functions of the ipsilateral and contralateral spinoparabrachial pathways. We also demonstrated the major downstream target of PBN neurons that receive spinal input and identified the major subtype of neurons in the PBN that is involved in the processing of nociceptive information.

RESULTS

Synaptic Connection Pattern of the Spinoparabrachial Pathway

Spinal projection neurons send projections to multiple brain areas, including the thalamus, periaqueductal gray (PAG), and PBN (Al-Khater and Todd, 2009; Gauriau and Bernard, 2004; Todd, 2010). The PBN receives bilateral input from spinal projection neurons (Spike et al., 2003). However, the pattern of functional connectivity of the spinoparabrachial pathway remains unknown. We addressed this issue with viral tracing and electrophysiological approaches. We labeled the spinal neurons, including projection neurons, by injecting AAV2/9-hSyn-hChR2(H134R)-mCherry virus into the right dorsal spinal cord of wild-type mice (Figures 1A and S1A). Consistent with previous studies (Feil and Herbert, 1995; Gauriau and Bernard, 2004), mCherry$^+$ fibers originating from the spinal cord were observed in multiple brain areas, including the PBN, thalamus, and PAG (Figures 1B and S1B–S1E). In many brain areas, mCherry$^+$ fibers were mostly located in the contralateral side. In contrast, abundant mCherry$^+$ fibers were observed in both the ipsilateral and contralateral PBN, and most of the mCherry$^+$ fibers were located in the superior lateral part of the PBN (PBNsl) (Figure 1B). After summarizing mCherry$^+$ fibers from three mice, we found that the distribution pattern of mCherry$^+$ fibers was slightly different between the ipsilateral and contralateral sides, with more mCherry$^+$ fibers on the contralateral side of the rostral PBN but more in the ipsilateral side of the caudal PBN (Figure 1C). As the mCherry$^+$ fibers could be fibers of passage, we further examined the distribution pattern of presynaptic terminals of the spinoparabrachial projection by employing AAV2/8-hSyn-DIO-Synaptophysin-tdTomato virus, which labels presynaptic terminals with tdTomato in a Cre-dependent manner (Cao et al., 2020). As most spinal projection neurons are vesicular glutamate transporter 2 (*Vglut2*)-positive neurons (Todd, 2010), we injected this virus into the superficial layer of the dorsal spinal cord of *Vglut2-Cre* mice (Figure S1F). We analyzed the distribution pattern of presynaptic terminals labeled with tdTomato and observed similar results (Figures S1G-S1I3).

Next, we examined functional synaptic connectivity and properties of the spinoparabrachial pathway with whole-cell patch-clamp recording. We recorded PBN neurons in acute slices prepared from mice that were injected with AAV2/9-hSyn-hChR2(H134R)-mCherry virus in the right side of dorsal spinal cord (Figure 1D). We found that optogenetic activation of the spinoparabrachial fibers evoked excitatory postsynaptic currents (EPSCs) (Figure 1E) in a small percentage of PBN neurons, consistent with recent studies (Chiang et al., 2020; Huang et al., 2019; Mu et al., 2017). The average latency of EPSCs was 2.6 ± 0.9 ms for the contralateral PBN (with jitter of 0.11 ± 1.16 ms) and 2.4 ± 1.1 ms for the ipsilateral PBN (with jitter of 0.11 ± 0.08 ms), indicating monosynaptic connections. The amplitude of the EPSCs was slightly higher in the ipsilateral PBN (Figure 1F), but the connection rates were comparable (contralateral, 0.23; ipsilateral, 0.26). We plotted the location of all recorded neurons and found that most PBN neurons responding to optogenetic stimulation of spinoparabrachial fibers were located in the PBNsl (Figure 1G), consistent with the viral tracing results presented above. To systematically map PBN neurons that receive spinal inputs, we employed AAV2/1-CMV-bGlobin-Cre-EGFP virus, which could anterogradely label postsynaptic targets of the infected neurons with Cre recombinase (Zingg et al., 2017). We injected this virus into the dorsal spinal cord of Ai9 mice (Figure S1J) and analyzed the distribution pattern of tdTomato$^+$ PBN neurons that received projections from the spinal cord (hereafter referred to as PBN_{SC} neurons). We found that tdTomato$^+$ neurons were located in both the ipsilateral and contralateral PBNsl (Figures S1K-S1M3) and that their distribution pattern was similar to that obtained in the slice

(S) Changes of fluorescent signal of GCaMP6s expressed in PBN neurons evoked by noxious cold stimulation (n = 6 mice, blue lines, response for individual mouse; red line, average response).
(T) Summary of average fluorescent signal of GCaMP6s expressed in PBN neurons evoked by noxious cold stimulation (n = 6 mice, paired Student's t test).
(U) Schematic showing recording of PBN neurons in response to foot shock (0.3 mA, 2 s).
(V) Changes of fluorescent signal of GCaMP6s expressed in PBN neurons evoked by foot shock (blue lines, response for individual mouse; red line, average response).
(W) Summary of average fluorescence changes in PBN neurons evoked by foot shock stimulation (n = 6 mice, paired Student's t test).
*p < 0.05 and **p < 0.01. Error bars represent SEMs, shaded areas indicate SEMs. See also Figure S1.

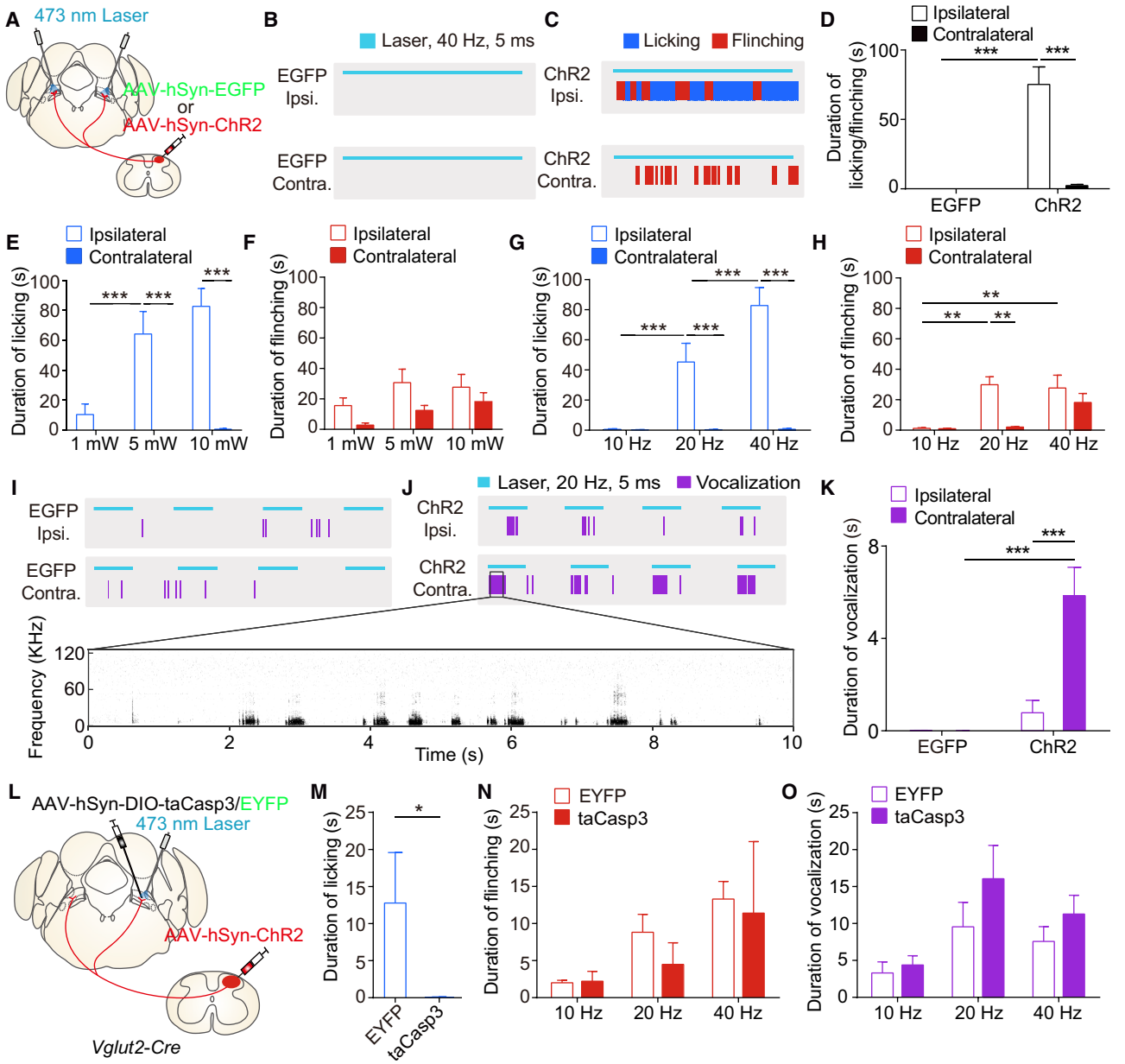

Figure 2. Activation of the Spinoparabrachial Pathway Evoked Pain-Related Behaviors

(A) Schematic for viral injection in the spinal cord and optical fiber implantation above the PBN.

(B) Raster plot showing behaviors evoked by photostimulation (473 nm, 20 Hz, 10 mW, 30 s) in a mouse injected with AAV2/9-hSyn-EGFP virus.

(C) Raster plot showing behaviors evoked by photostimulation (473 nm, 20 Hz, 10 mW, 30 s) in a mouse injected with AAV2/9-hSyn-hChR2(H134R)-mCherry virus.

(D) Duration of licking and flinching behaviors responding to photostimulation (473 nm, 20 Hz, 10 mW, n = 7–11 mice, two-way ANOVA).

(E and F) Duration of licking (E) and flinching (F) behaviors with photostimulation (473 nm, 40 Hz) under different light intensities (n = 9–11 mice, two-way ANOVA).

(G and H) Duration of licking (G) and flinching (H) behaviors with photostimulation (473 nm, 10 mW) under different frequencies (n = 9–11 mice, two-way ANOVA).

(I) Raster plot showing vocalization evoked by photostimulation (473 nm, 20 Hz, 10 mW, 30 s) in a mouse injected with AAV2/9-hSyn-EGFP virus.

(J) Top: raster plot showing vocalization evoked by photostimulation (473 nm, 20 Hz, 10 mW, 30 s) in a mouse injected with AAV2/9-hSyn-hChR2(H134R)-mCherry virus. Bottom: the pattern of vocalization of the boxed duration.

(K) Duration of vocalization recorded during activation of ipsilateral or contralateral pathway with photostimulation (473 nm, 20 Hz, 10 mW, n = 8–11 mice, two-way ANOVA).

(L) Schematic depicting viral injection in the spinal cord and PBN and optical fiber implantation above the PBN.

(legend continued on next page)

electrophysiology experiment. We summarized the density of tdTomato$^+$ neurons from three mice and found more postsynaptic neurons on the ipsilateral side of the caudal PBN (Figures S1L1-S1M3). Together, our data suggest that neurons in the spinal cord form bilateral functional connections with the PBNsl with slightly different patterns.

Activation of the PBNsl by Noxious Stimuli

Given that neurons receiving spinal input are mostly located in the PBNsl and that neurons in this area were shown to be activated by noxious stimuli (Bourgeais et al., 2001), we determined the potential involvement of the spinoparabrachial pathway in processing nociceptive information by recording the response of the PBNsl to noxious stimuli with GCaMP6s (Gunaydin et al., 2014). We injected AAV2/9-hSyn-GCaMP6s virus into the PBN and implanted optical fibers above the PBNsl to measure the activity of PBNsl neurons with fiber photometry, and AAV2/9-hSyn-EGFP virus was injected as a control (Figures 1H and S1N). We found that noxious mechanical stimuli (pinch) activated PBNsl neurons, as evidenced by the significantly elevated fluorescent signal for GCaMP6s (Figures 1I–1L). In contrast, the fluorescent signal for EGFP in the control mice did not change significantly (Figures 1I, 1K, and 1L). To test whether neurons in the PBNsl could respond to noxious stimuli applied to other parts of the body, we examined the response of PBNsl neurons to mechanical stimulation applied to the paws and found that neurons in the PBNsl were also activated by pinching paws (Figures 1M and S1O). Next, we tested whether PBNsl neurons are activated by noxious thermal stimulation (Figure 1N). We found that these neurons were activated by noxious thermal stimulation applied to the tail (46°C and 52°C) (Figures 1O–1Q, S1P, and S1Q), but not by innocuous thermal stimulation (40°C) (Figures 1O–1Q), indicating that PBNsl neurons are selectively activated by noxious thermal stimulation. Further, we found that PBNsl neurons were activated by noxious cold stimulation applied to the hind paw (Figures 1R–1T, S1R, and S1S).

The experiments above were all performed under anesthesia. We further defined the response of PBNsl neurons to noxious stimulation in awake animals and found that the activity of PBNsl neurons increased significantly in response to foot shock (Figures 1U–1W, S1T, and S1U). Accordingly, the activity of PBNsl neurons also increased when animals were placed on a hot plate set to 56°C; however, the response of PBNsl neurons did not change significantly when the animals were placed on a hot plate set to 40°C or 48°C (Figures S1V and S1W). Thus, neurons in the PBNsl are activated by numerous noxious stimuli.

Functional Roles of the Spinoparabrachial Pathway in Nociception

Although the spinoparabrachial pathway has long been thought to be involved in nociceptive information processing (Bester et al., 1997, 2000; Williams and Ivanusic, 2008), the functional role of this pathway remains largely unknown. Using optogenetic approaches, we examined the potential functional role of the spinoparabrachial pathway in nociception. To directly manipulate the spinoparabrachial pathway, we injected AAV2/9-hSyn-hChR2(H134R)-mCherry or AAV2/8-hSyn-EGFP virus into the right dorsal spinal cord and implanted optical fibers bilaterally above the PBN (Figure 2A). We found that photostimulation of the ipsilateral spinoparabrachial pathway induced robust pain-related licking and flinching behaviors of the right hind paw, but no pain-related behaviors were detected in control mice under the same manipulation (Figures 2B–2D). In contrast, photostimulation of the contralateral spinoparabrachial pathway evoked significantly less licking and flinching behaviors of the right hind paw (Figures 2C and 2D). The duration of licking and flinching behaviors evoked following activation of the ipsilateral spinoparabrachial pathway increased when the frequency or power of the photostimulation increased (Figure S2A). Similar results were observed on the left hind paw when the ipsilateral or contralateral spinoparabrachial pathway originating from the left dorsal spinal cord was manipulated (Figure S2B). A recent study indicated that licking and flinching behaviors could be mediated by distinct mechanisms (Huang et al., 2019). We thus analyzed the licking and flinching behaviors separately. The duration of licking behaviors induced by photoactivation of the ipsilateral spinoparabrachial pathway was significantly longer than that evoked following activation of the contralateral pathway under most conditions (Figures 2E and 2G). In contrast, the duration of flinching behaviors evoked following activation of the ipsi- and contralateral pathways was comparable under most conditions, except stimulation at 20 Hz and 10 mW (Figures 2F and 2H). These data support the idea that these two behavioral responses could be mediated by different mechanisms. Interestingly, activation of the contralateral spinoparabrachial pathway evoked significantly more vocalization than that of the ipsilateral pathway, likely reflecting the pain-associated negative affect (Figures 2I–2K), as suggested previously (Rodriguez et al., 2017). These data indicate that the ipsilateral and contralateral spinoparabrachial pathways play distinct roles in processing nociceptive information.

Spinal neurons projecting to the PBN may also project to other brain areas (Al-Khater and Todd, 2009; Hylden et al., 1989; Spike et al., 2003). Thus, the behavioral responses evoked by optogenetic activation of the spinoparabrachial pathway might have resulted from activation of other pathways. To address this issue, we tested whether ablation of *Vglut2*$^+$ PBN neurons, which are the most abundant neurons in the PBN (Mu et al., 2017), would abolish behavioral responses evoked following activation of the spinoparabrachial pathway. We injected AAV2/9-hSyn-hChR2(H134R)-mCherry virus into the right dorsal spinal cord of *Vglut2-Cre* mice, followed by injecting AAV2/9-CAG-DIO-taCasp3-TEVp or AAV2/9-EF1α-DIO-EYFP virus into the ipsilateral PBN (Figure 2L). This manipulation led to the ablation of *Vglut2*$^+$

(M) Duration of licking behavior responding to photostimulation (473 nm, 10 mW, 40 Hz) of ipsilateral spinoparabrachial pathway (n = 9–12 mice, unpaired Student's t test).
(N) Duration of flinching behavior responding to photostimulation (473 nm, 10 mW) of ipsilateral spinoparabrachial pathway (n = 9–12 mice, two-way ANOVA).
(O) Duration of vocalization recorded responding to photostimulation (473 nm, 10 mW) of contralateral pathway (n = 6–10 mice, two-way ANOVA).
Ipsi., ipsilateral; Contra., contralateral. *$p < 0.05$, **$p < 0.01$, and ***$p < 0.001$. Error bars represent SEMs. See also Figure S2.

neurons in the ipsilateral PBN (Figures S2C–S2E). We found that the ablation of *Vglut2*$^+$ PBN neurons decreased light-evoked pain-related licking behaviors compared with that observed in the control mice (Figure 2M), but light-evoked flinching behaviors were not significantly affected (Figure 2N). These results support the idea that the PBN was actively involved in licking behaviors evoked following activation of the ipsilateral spinoparabrachial pathway. In contrast, vocalization following photostimulation of the spinal projection fibers in the contralateral PBN was not affected after ablation of *Vglut2*$^+$ neurons in the contralateral PBN (Figures 2O, S2F, and S2G). Thus, vocalization following photostimulation of the contralateral spinoparabrachial pathway could have resulted from the activation of passing spinal projection fibers in the PBN that target other brain areas.

The PBN is thought to be involved in mediating the negative affective component of pain, which is supported by several recent studies showing that activation of the craniofacial-PBN pathway or spinal input to the PBN induced real-time place aversion (RTPA) (Huang et al., 2019; Rodriguez et al., 2017). We thus further determined the potential role of the ipsilateral or contralateral spinoparabrachial pathway in driving avoidance behaviors with the RT-PA test (Figures S2H, S2I, and S2L). We found that ChR2-expressing mice spent significantly more time in the unstimulated side after optogenetic activation of ipsilateral or contralateral pathway (Figures S2J and S2M). We compared the avoidance scores (time spent in the stimulated side during the light stimulation period minus that during the unstimulated period) after activation of these two pathways and found that activation of the contralateral pathway evoked a higher avoidance score than that of the ipsilateral pathway (Figure S2N). However, the ablation of *Vglut2*$^+$ PBN neurons had no significant effect on the avoidance behaviors evoked following activation of the ipsilateral (Figure S2K) or contralateral spinoparabrachial pathway (Figure S2O). These data suggest that PBN neurons play a minor role in mediating the avoidance behaviors evoked by the activation of fibers originating from the spinal cord.

The Ipsilateral Spinoparabrachial Pathway Is Necessary for Nociceptive Information Processing

We next asked whether the spinoparabrachial pathway is necessary for the processing of nociceptive information. Given that mice with inflammatory pain induced by intraplantar injection of formalin exhibit robust licking and flinching behaviors, we tested whether suppression of the spinoparabrachial pathway would impair formalin-induced licking and flinching behaviors. We employed the designer receptors exclusively activated by a designer drug (DREADD) system (Armbruster et al., 2007) to manipulate the activity of the spinoparabrachial pathway (Figures 3A, S3A, and S3B). We found that pharmacogenetic suppression of the ipsilateral spinoparabrachial pathway significantly decreased the duration of licking behaviors in the second phase of the formalin test, but not in the first phase (Figures 3B, 3C, and 3E). This manipulation did not significantly affect formalin-evoked flinching behaviors (Figures 3B, 3D, and 3F). By contrast, we found that pharmacogenetic inhibition of the contralateral spinoparabrachial pathway had no significant effect on formalin-evoked licking or flinching behaviors (Figures 3G–3J, S3C, and S3D). These data suggest that the ipsilateral spinoparabrachial pathway rather than the contralateral spinoparabrachial pathway is necessary to generate nocifensive behavior.

To further confirm the functional role of the spinoparabrachial pathway, we selectively manipulated the activity of PBN_{SC} neurons by employing AAV2/1-CMV-bGlobin-Cre-EGFP virus, which can anterogradely infect the postsynaptic partners of infected neurons (Zingg et al., 2017). We injected AAV2/1-CMV-bGlobin-Cre-EGFP virus into the right spinal cord and AAV2/5-hSyn-DIO-hM4Di-mCherry or AAV2/9-EF1α-DIO-EYFP virus into the ipsilateral PBN for manipulating the ipsilateral PBN_{SC} neurons (Figure 3K). We found that licking behaviors, but not flinching behaviors, were significantly decreased in hM4Di-expressing mice after intraperitoneal Clozapine-n-oxide (CNO) injection compared with control mice (Figures 3L–3N). In contrast, formalin-evoked pain-related behaviors were not significantly affected by the suppression of contralateral PBN_{SC} neurons (Figures S3E–S3H). Together, these results suggest that the ipsilateral spinoparabrachial pathway rather than the contralateral spinoparabrachial pathway is necessary for formalin-evoked pain-related licking behaviors.

Tacr1-Positive Neurons in the PBN Play an Important Role in Processing Nociceptive Information

There are multiple subtypes of neurons in the PBN (Maeda et al., 2009). To further define the cell type of PBN_{SC} neurons, we labeled PBN_{SC} neurons with GFP by injecting an anterogradely transporting virus, AAV2/1-hSyn-Flpo, into the dorsal spinal cord of H2B-GFP mice (Figures 4A and S4A), which expressed GFP in a Flpo-dependent manner (He et al., 2016). Next, we examined the expression of *CGRP*, somatostatin (*Sst*), *Pdyn*, and tachykinin receptor 1 (*Tacr1*) in GFP-labeled PBN_{SC} neurons. We found that among markers tested, *Tacr1*$^+$ neurons exhibited the highest overlapping percentage with PBN_{SC} neurons (Figures 4B–4D) and showed a distribution pattern similar to that of PBN_{SC} neurons. In contrast, PBN_{SC} neurons showed limited overlap with *CGRP*$^+$, *Pdyn*$^+$, or *Sst*$^+$ neurons in the PBN (Figures 4D and S4B1–S4B3). Thus, *Tacr1*$^+$ neurons in the PBN represent a major target of the spinoparabrachial projection.

To examine the functional role of *Tacr1*$^+$ PBN neurons in nociceptive information processing, we generated a *Tacr1-flpo* mouse line in which *Tacr1*$^+$ neurons were labeled with high specificity, although only approximately half of the *Tacr1*$^+$ neurons were labeled (Figures S4C–S4F). To inhibit the neuronal activity of *Tacr1*$^+$ neurons in the PBN with pharmacogenetic approaches, we injected AAV2/9-EF1α-fDIO-hM4Di-mCherry or AAV-EF1α-fDIO-mCherry virus into the right PBN of *Tacr1-flpo* mice (Figures 4E and 4F). We found that pharmacogenetic suppression of *Tacr1*$^+$ neurons in the ipsilateral PBN significantly reduced the duration of formalin-evoked licking behaviors, but not flinching behaviors, compared with that of the control group (Figures 4G and 4H). In contrast, ablation of either *Sst*$^+$ or *Pdyn*$^+$ PBN neurons had no significant effect on formalin-evoked licking or flinching behaviors (Figures S4G–S4N). These data indicate that *Tacr1*$^+$ neurons in the PBN are necessary for formalin-evoked licking behaviors.

Next, we determined whether pharmacogenetic activation of *Tacr1*$^+$ neurons in the PBN would induce spontaneous

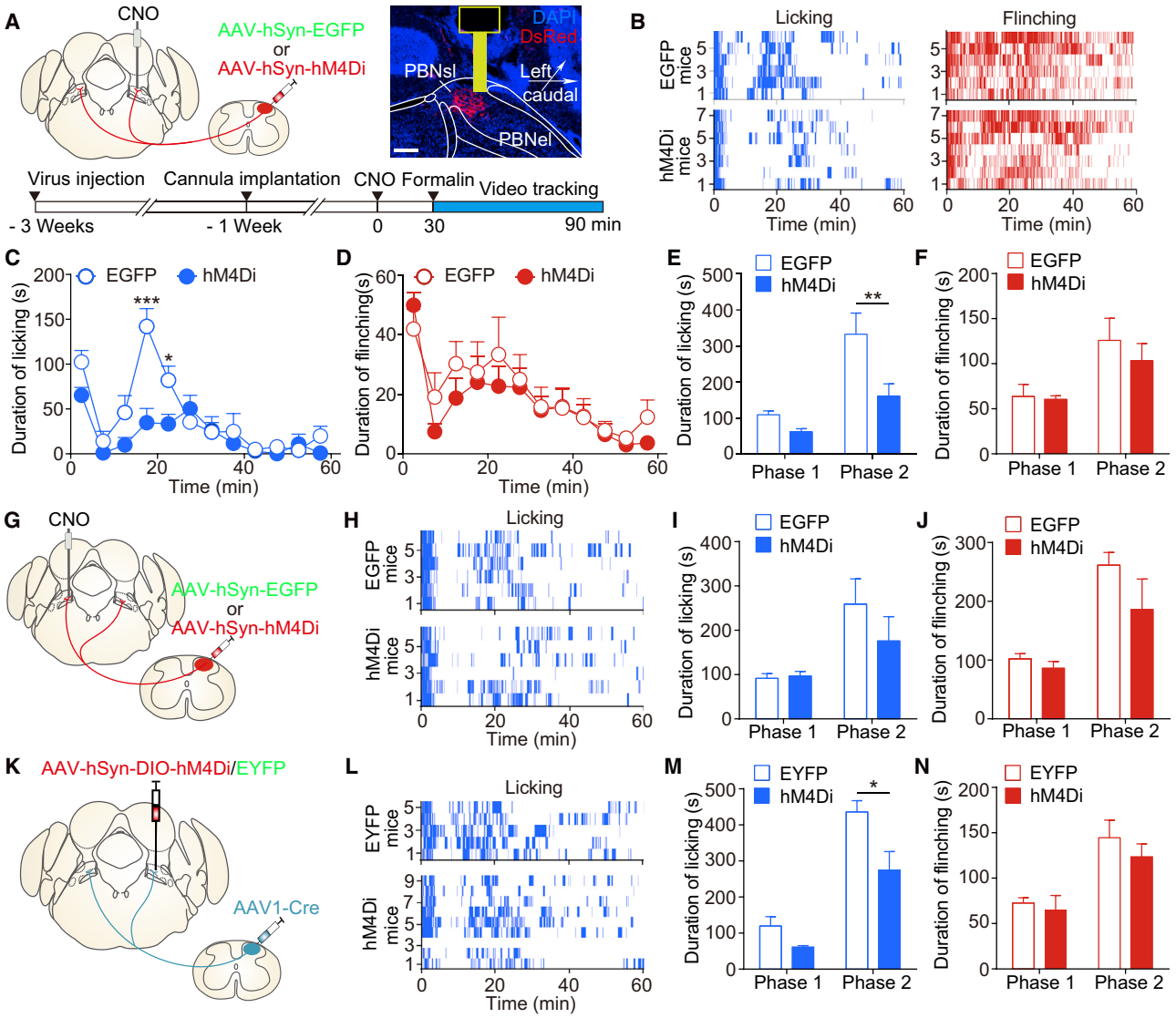

Figure 3. Inhibition of the Ipsilateral Spinoparabrachial Pathway Impaired Formalin-Evoked Pain-Related Behaviors

(A) Top left: schematic for virus injection in spinal cord and cannula implantation above PBN. Top right: distribution of hM4Di-positive fibers and track of cannula in the PBN. Yellow line, outer and injection cannula. Scale bar, 200 μm. Bottom: timeline of the experiment.

(B) Raster plot showing formalin-evoked behaviors after CNO injection into the ipsilateral PBN (0.5 μg/mouse).

(C and D) Graph showing formalin-evoked licking (C) and flinching (D) behaviors after CNO injection (n = 6–7 mice, unpaired Student's t test).

(E and F) Duration of formalin-evoked licking (E) and flinching (F) behaviors after CNO injection (n = 6–7 mice, two-way ANOVA).

(G) Schematic depicting viral injection into the right dorsal spinal cord and cannula implantation above the contralateral PBN of wild-type mice.

(H) Raster plot showing formalin-evoked licking behavior after CNO injection into the contralateral PBN (0.5 μg/mouse).

(I and J) Duration of formalin-evoked licking (I) and flinching (J) behaviors after CNO injection into the contralateral PBN (n = 6 mice, two-way ANOVA).

(K) Schematic showing viral injection into the right dorsal spinal cord and ipsilateral PBN of wild-type mice.

(L) Raster plot showing formalin-evoked licking behavior after CNO injection (1 mg/kg, intraperitoneally [i.p.]).

(M and N) Duration of formalin-evoked licking (M) and flinching (N) behaviors after CNO injection (n = 5–9 mice, two-way ANOVA)

*p < 0.05, **p < 0.01. Error bars represent SEMs. See also Figure S3.

nocifensive behaviors (Figures 4I, 4J, and S4O). Pharmacogenetic activation of *Tacr1*$^+$ neurons in the PBN evoked robust spontaneous licking behaviors (Figures 4K, 4L, and S4Q). In contrast to the results obtained following activation of the spinoparabrachial pathway, we observed spontaneous licking behaviors on both the ipsilateral and contralateral hind paws after activating *Tacr1*$^+$ neurons in the right PBN (Figures 4L and S4Q). No significant difference was observed for duration of flinching behaviors in the ipsilateral (Figure S4P) or contralateral (Figure S4R) hind paw between hM3Dq-expressing mice and control mice. These data suggest that the activation of *Tacr1*$^+$ neurons in the PBN is sufficient to generate pain-related licking behaviors.

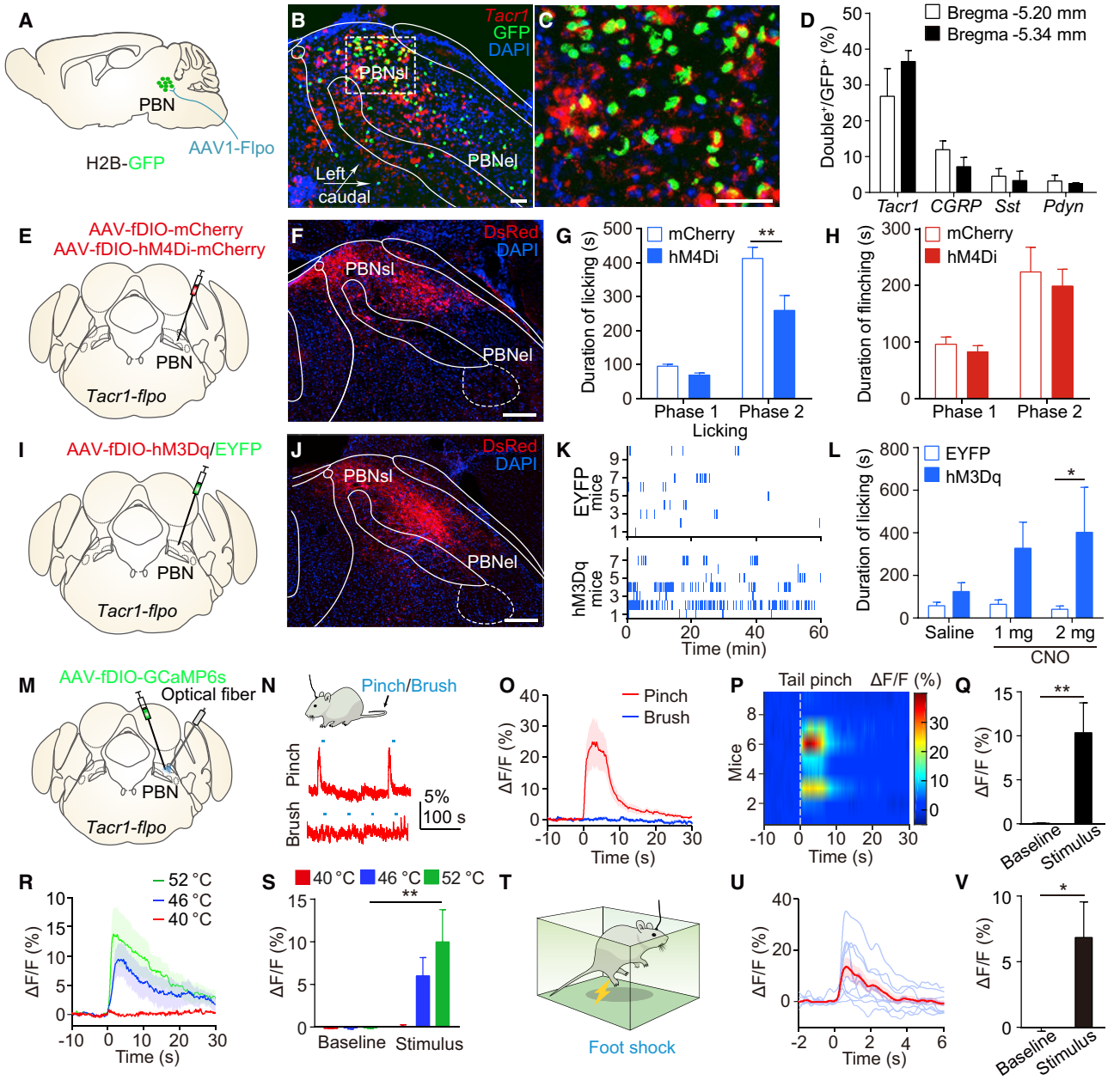

Figure 4. Functional Roles of *Tacr1*$^+$ PBN Neurons in Processing Nociceptive Information

(A) Schematic for labeling PBN_{SC} neurons in H2B-GFP mice.

(B) Distribution pattern of GFP$^+$ (green) and *Tacr1*$^+$ (red) neurons in the PBN. Scale bar, 50 μm.

(C) Magnified view of the boxed area in (B). Scale bar, 50 μm.

(D) Percentage of different cell types among GFP$^+$ neurons (n = 3–4 mice).

(E) Schematic showing viral injection into the right PBN of *Tacr1-flpo* mice.

(F) Distribution pattern of hM4Di$^+$ (DsRed) neurons in the right PBN. Scale bar, 200 μm.

(G and H) Duration of formalin-evoked licking (G) and flinching (H) behaviors after CNO injection (1 mg/kg, i.p.) (n = 7–8 mice, two-way ANOVA).

(I) Schematic showing viral injection into right PBN of *Tacr1-flpo* mice.

(J) Distribution pattern of hM3Dq$^+$ (DsRed) neurons in the right PBN. Scale bar, 200 μm.

(K) Raster plot showing CNO-evoked licking behavior on right hind paw after CNO injection (2 mg/kg, i.p.).

(L) Duration of licking behavior on right hind paw after saline or CNO injection (i.p.) (n = 6–10 mice, two-way ANOVA).

(M) Schematic showing viral injection and optical fiber implantation in *Tacr1-flpo* mice.

(N) Top: schematic showing recording of *Tacr1*$^+$ PBN neurons in response to mechanical stimulation. Bottom: raw traces of fluorescent GCaMP6s signal of *Tacr1*$^+$ PBN neurons in response to pinch or brush stimulation. Blue bars indicate pinch (5 s) or brush (3 s) stimulation.

(legend continued on next page)

We next examined whether *Tacr1*$^+$ neurons in the PBN could be activated by noxious stimulation with fiber photometry (Figure 4M). We defined the response of *Tacr1*$^+$ neurons to mechanical stimulation (Figure 4N) and found that noxious mechanical stimulation (pinch), but not innocuous stimulation (brush), applied to the tail increased the activity of *Tacr1*$^+$ neurons (Figures 4N–4Q, S4S, and S4T). Next, we measured the activity of *Tacr1*$^+$ neurons in response to thermal stimulation. We found that *Tacr1*$^+$ neurons were activated by noxious thermal stimulation (46°C and 52°C), but not by innocuous thermal stimulation (40°C) (Figures 4R, 4S, S4U, and S4V). *Tacr1*$^+$ neurons in the PBN were also activated by noxious cold stimulation (Figures S4W and S4X). In addition, *Tacr1*$^+$ neurons in the PBN were activated by foot shock under the awake state (Figures 4T–4V, S4Y, and S4Z). Thus, *Tacr1*$^+$ neurons in the PBN are activated by noxious stimuli.

Indirect Connection between PBN_{SC} Neurons and the CeA

It has been long thought that PBN_{SC} neurons send direct projections to the CeA. We tested this with neural tracing and electrophysiological approaches, mainly focusing on the ipsilateral spinoparabrachial pathway. To examine the relationship between PBN_{SC} neurons and CeA-projecting PBN neurons (hereafter referred to as PBN_{CeA} neurons), we labeled PBN_{SC} and PBN_{CeA} neurons in H2B-GFP mice by injecting AAV2/1-hSyn-Flpo virus into the spinal cord and Red-beads into CeA (Figure 5A). Surprisingly, little colocalization (ranging from 2.77% to 9.52%) between PBN_{SC} neurons (GFP$^+$) and PBN_{CeA} neurons (Red-beads$^+$) (Figures 5B–5D) was detected, indicating that PBN_{SC} and PBN_{CeA} neurons are largely nonoverlapping. This result was also confirmed with the retrograde tracer CTB-555 (colocalization, ranging from 0 to 3.7%; Figures 5A and 5E–5G). We also tested the colocalization of PBN_{SC} and PBN_{CeA} neurons with retrograde rAAV2/2-retro-CMV-bGlobin-Cre-EGFP virus (Tervo et al., 2016). In H2B-GFP mice, we injected anterograde AAV2/1-hSyn-Flpo virus into the spinal cord to label PBN_{SC} neurons, retrograde rAAV2/2-retro-CMV-bGlobin-Cre-EGFP virus into the CeA, and AAV2/8-hSyn-DIO-mCherry into the PBN to label PBN_{CeA} neurons, respectively (Figure S5A), and found limited colocalization (ranging from 6.84% to 22%) between PBN_{SC} neurons (GFP$^+$) and PBN_{CeA} neurons (mCherry$^+$) (Figures S5B–S5D). The variation in percentage of colocalization among different approaches may be due to different diffusion property of the tracers. Thus, PBN_{SC} and PBN_{CeA} neurons are largely nonoverlapping, indicating that PBN_{SC} neurons send limited direct projections to the CeA.

To examine the projection pattern of PBN_{SC} neurons and identify the major downstream target of PBN_{SC} neurons, we labeled PBN_{SC} neurons with EYFP by injecting AAV2/1-CMV-bGlobin-Cre-EGFP virus into the dorsal spinal cord and AAV2/9-EF1α-DIO-EYFP virus into the ipsilateral PBN (Figure 5H) and examined the distribution pattern of EYFP$^+$ fibers in the brain. We detected EYFP$^+$ fibers in many brain areas, including the ILN, PAG, intermediate gray layer of the superior colliculus (InG), CeA, and bed nucleus of stria terminalis (BNST) (Figures 5I–5N), with the most abundant EYFP$^+$ fibers in the ILN (Figure 5J).

Although the EYFP$^+$ fibers observed in the CeA were relatively sparse (Figures 5K and S5E–S5J), this small number of fibers may form strong functional synapses with CeA neurons. To further examine this possibility, we selectively expressed ChR2 in PBN_{SC} neurons and recorded CeA neurons from these animals with slice electrophysiology (Figures 5O and 5P). Photostimulation of ChR2-positive PBN neurons evoked reliable action potentials (Figure 5Q). However, we detected no light-evoked excitatory (0 out of 25 neurons, n = 4 mice) or inhibitory (0 out of 25 neurons, n = 4 mice) postsynaptic responses in CeA neurons (Figure 5R). These data indicate that PBN_{SC} neurons send very few, if any, direct functional projections to CeA neurons.

It has been suggested that the local circuit is important for relaying information from PBN_{SC} neurons to PBN_{CeA} neurons (Chiang et al., 2020). We asked whether PBN_{SC} neurons send signals to CeA indirectly via the local connection between PBN_{SC} and PBN_{CeA} neurons. To test this possibility, we selectively expressed ChR2 in PBN_{SC} neurons and retrogradely labeled PBN_{CeA} neurons with Green-beads (Figure S5K). By recording from Green-beads$^+$ PBN_{CeA} neurons (Figures S5L1–S5L4), we found that photostimulation of PBN_{SC} neurons evoked both excitatory (3 out of 36 neurons, average amplitude: 26.4 ± 16.3 pA) and inhibitory (7 out of 36 neurons, average amplitude: 22.8 ± 8.4 pA) postsynaptic responses in Green-beads$^+$ PBN_{CeA} neurons with short latency (3.0 ± 1.6 ms for EPSCs and 3.5 ± 0.9 ms for IPSCs; Figures S5M–S5R), indicating direct synaptic connection. Together, our data suggest that PBN_{SC} neurons can send spinal information to CeA via indirect connections between PBN_{SC} and PBN_{CeA} neurons.

Functional Connection between PBN_{SC} Neurons and the ILN

Projections from the PBN to the ILN have been implicated in processing nociceptive information (Bourgeais et al., 2001), which is consistent with our results showing that PBN_{SC} neurons send dense projections to the ILN (Figure 5J). We further confirmed this by employing the retrograde tracing method and found that ILN-projecting neurons in the PBN (hereafter referred to as PBN_{ILN}) labeled with retrograde Red-beads were located in a

(O) Average fluorescent signal of GCaMP6s expressed in the *Tacr1*$^+$ PBN neurons evoked by pinch or brush stimulation (n = 9 mice).
(P) Heatmap showing the calcium response of *Tacr1*$^+$ PBN neurons to tail pinch stimulation.
(Q) Summary of average fluorescence changes in *Tacr1*$^+$ PBN neurons evoked by tail pinch stimulation (n = 9 mice, paired Student's t test).
(R) Average fluorescent signal of GCaMP6s expressed in the *Tacr1*$^+$ PBN neurons evoked by thermal stimulation (tail immersion in water). (n = 2–6 mice).
(S) Summary of average fluorescent calcium responses of *Tacr1*$^+$ PBN neurons evoked by thermal stimulation (n = 2–6 mice, two-way ANOVA).
(T) Schematic showing recording of *Tacr1*$^+$ PBN neurons in response to foot shock (0.3 mA, 2 s).
(U) Changes of fluorescent signal of GCaMP6s expressed in the *Tacr1*$^+$ PBN neurons evoked by foot shock stimulation. Blue line, response for individual mouse; red line, average response.
(V) Summary of average fluorescent calcium changes in *Tacr1*$^+$ PBN neurons evoked by foot shock (n = 9 mice, paired Student's t test).
*p < 0.05, **p < 0.01. Error bars represent SEMs, shaded areas indicate SEMs. See also Figure S4.

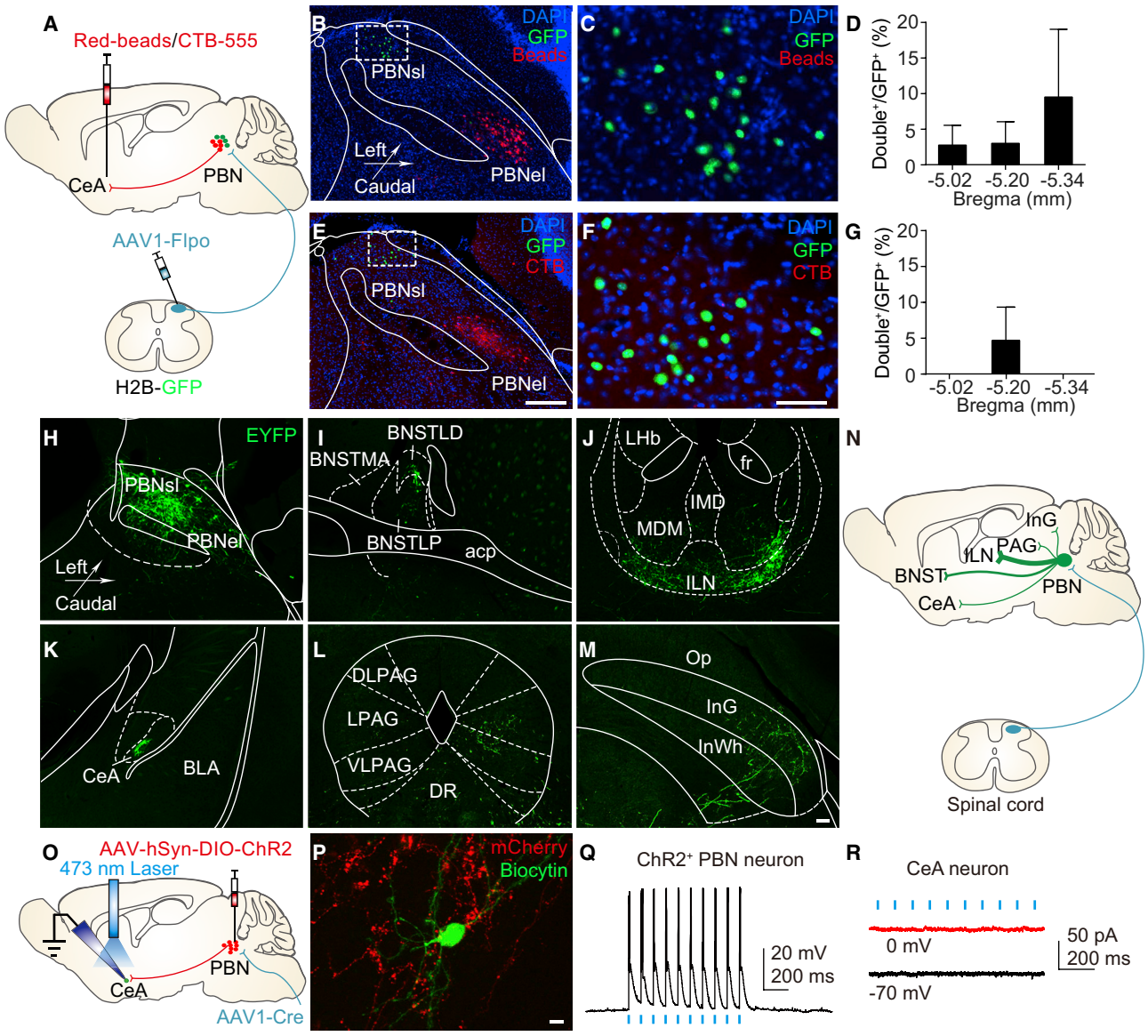

Figure 5. PBN_{SC} Neurons Sent Limited Direct Projections to the CeA

(A) Schematic showing viral injection into the right dorsal spinal cord and Red-beads/CTB-555 into CeA of H2B-GFP mice.
(B) Distribution pattern of GFP^+ (green) and Red-$beads^+$ (red) neurons in the PBN.
(C) Magnified view of the boxed area in (B).
(D) Percentage of double labeled neurons among GFP^+ neurons (n = 3 mice).
(E) Distribution pattern of GFP^+ (green) and $CTB\text{-}555^+$ (red) neurons in the PBN. Scale bar, 200 μm.
(F) Magnified view of the boxed area in (E). Scale bar, 50 μm.
(G) Percentage of double labeled neurons among GFP^+ neurons (n = 3 mice).
(H–M) Distribution patterns of $EYFP^+$ neurons/fibers in the PBN (H), BNST (I), ILN (J), CeA (K), PAG (L), and InG (M) of an example mouse received injection of AAV2/9-EF1α-DIO-EYFP virus into the right PBN and AAV2/1-CMV-Cre-EGFP virus into the right dorsal spinal cord. Scale bar, 100 μm.
(N) Schematic showing summary of the distribution pattern of $EYFP^+$ fibers from PBN_{SC} neurons.
(O) Schematic showing viral injection into the spinal cord and PBN and electrophysiological recording of CeA neurons of wild-type mice.
(P) Detection of $Biocytin^+$ (green) recorded neurons and $mCherry^+$ (red) ChR2 fibers in CeA. Scale bar, 10 μm.
(Q) Light-evoked action potentials recorded in a $ChR2^+$ PBN neuron. Blue bars indicate photostimulation (473 nm, 1 ms).
(R) No response was recorded in CeA neurons at 0 mV or −70 mV after photostimulation. Blue bars indicate photostimulation (473 nm, 1 ms).
Error bars represent SEMs. See also Figure S5.

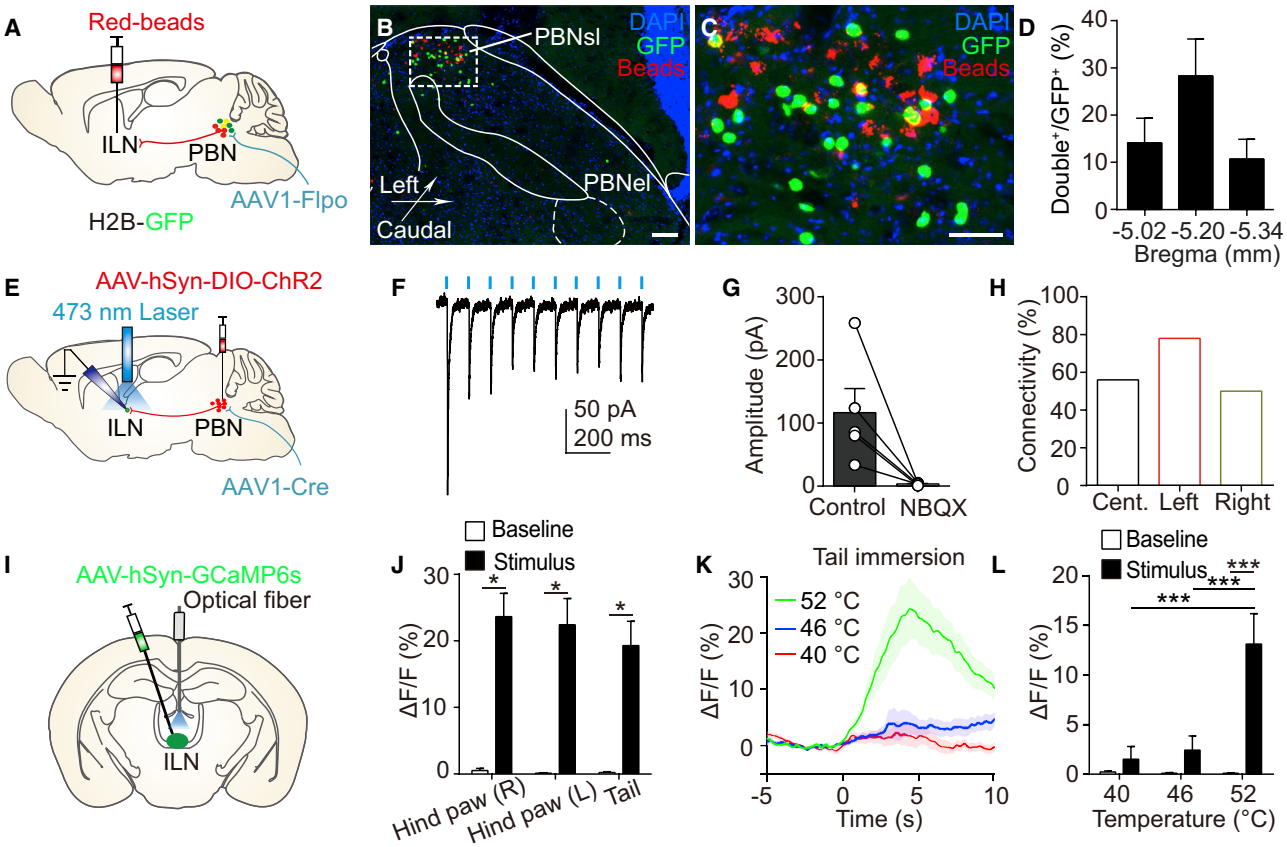

Figure 6. Functional Connection between PBN_{SC} Neurons and the ILN

(A) Schematic showing Red-beads injection into ILN and AAV2/1-hSyn-Flpo virus into the right spinal dorsal horn of H2B-GFP mice.
(B) Distribution pattern of GFP^+ (green) and Red-beads$^+$ (red) neurons in the PBN. Scale bar, 50 μm.
(C) Magnified view of the boxed area in (B). Scale bar, 50 μm.
(D) Percentage of double labeled neurons among GFP^+ neurons (n = 4 mice).
(E) Schematic showing viral injection into PBN, the right spinal dorsal horn and electrophysiological recording of ILN neurons of wild-type mice.
(F) Light-evoked inward currents recorded at −70 mV in an ILN neuron. Blue bars indicate photostimulation (473 nm, 1 ms).
(G) Light-evoked EPSCs were blocked after the application of NBQX, an antagonist of the AMPA receptor (n = 5 cells).
(H) Summary of the connectivity of light-evoked excitatory responses recorded in neurons located in different subareas of the ILN.
(I) Schematic showing viral injection into the ILN of wild-type mice. Optical fibers were implanted above the ILN.
(J) Summary of average fluorescent calcium changes in ILN neurons evoked by pinch stimulation (n = 6 mice, paired Student's t test).
(K) Changes of fluorescent signal of GCaMP6s expressed in the ILN in response to thermal stimulation (n = 4–6 mice, with shaded areas indicating SEMs).
(L) Summary of average fluorescent calcium changes in ILN neurons evoked by thermal stimulation (n = 4–6 mice, two-way ANOVA).
*p < 0.05, ***p < 0.001. Error bars represent SEMs. See also Figure S6.

subarea of PBN similar to that containing PBN_{SC} neurons (Figures 6A–6C). PBN_{ILN} neurons also exhibited higher colocalization with PBN_{SC} neurons (ranging from 11% to 29%) than that of PBN_{CeA} neurons (Figure 6D). We next examined the synaptic properties of the projections from PBN_{SC} neurons to ILN with slice recording. After selectively expressing ChR2 in PBN_{SC} neurons (Figure 6E and S6A), we recorded from neurons in the ILN and found that photoactivation of the fiber terminals of PBN_{SC} neurons in the ILN evoked EPSCs (21 out of 35 neurons, n = 4 mice) (Figure 6F). Moreover, the light-evoked EPSCs were blocked by bath application of the α-Amino-3-hydroxy-5-methyl-4-isoxazolepropionic acid (AMPA) receptor antagonist 2,3-Dioxo-6-nitro-1,2,3,4-tetrahydrobenzo[f]quinoxaline-7-sulfonamide (NBQX), suggesting that PBN_{SC} neurons form glutamatergic connections with neurons in the ILN (Figures 6G and S6B). The average latency for recorded EPSCs was less than 3 ms (Figure S6C), and the average jitter for the latency of recorded responses was 0.23 ms, indicating a monosynaptic connection. We plotted the location of all recorded neurons and found that the responsive neurons were located in the central medial, ipsilateral and contralateral paracentral nuclei of ILN (Figure S6D), and the connectivity was comparable for neurons located in the central and ipsilateral or contralateral area (Figure 6H). Together, these results suggest that PBN_{SC} neurons form strong functional glutamatergic synaptic connections with ILN neurons.

As the ILN receives dense projections from PBN_{SC} neurons, we hypothesized that ILN neurons would be activated by

noxious stimulation. To test this, we examined the response of ILN neurons to noxious stimulation (Figures 6I and S6E). We found that similar to PBNsl neurons, ILN neurons were activated by noxious mechanical stimulation (Figures 6J and S6F–S6H). We further examined whether ILN neurons could be activated by noxious thermal stimulation. Calcium signals of ILN neurons increased in response to noxious thermal stimulation (52°C; Figures 6K and 6L), which was similar to that observed in the PBN. Additionally, ILN neurons showed increased activity in response to noxious cold stimulation (Figures S6I, S6J, and S6M), foot shock (Figures S6K–S6M), and noxious thermal stimulation (Figures S6N–S6Q). Together, these data indicate that neurons in the ILN can be activated by noxious stimulation with a response pattern similar to that of the PBN, consistent with the notion that PBN-ILN projections play an important role in processing nociceptive signals.

DISCUSSION

Our study demonstrated that the spinoparabrachial pathway plays an important role in conveying nociceptive signals to the ILN rather than the CeA through disynaptic glutamatergic connections. We revealed that the ipsilateral spinoparabrachial pathway is sufficient and necessary for nocifensive behavior. We found that *Tacr1*$^+$ PBN neurons receive projections from the spinal cord and play important roles in nociception. Our study delineates the important neural circuit responsible for pain-related protective behaviors.

The Ipsilateral Spinoparabrachial Pathway Is Critical for Generating Nocifensive Behaviors

Although it has been shown that the spinal cord projects to both sides of the PBN (Hylden et al., 1989; Li and Li, 2000; Liu et al., 2009; Spike et al., 2003), the functional significance of the ipsilateral spinoparabrachial pathway remains unknown. We found that the ipsilateral spinoparabrachial pathway plays a key role in processing nociceptive information, which is supported by a recent study showing that the PBN plays an important role in inflammatory pain (Alhadeff et al., 2018). Together with previous studies (Bernard et al., 1996; Campos et al., 2018; Han et al., 2015; Menendez et al., 1996; Rodriguez et al., 2017), our results support the notion that the PBN and spinoparabrachial pathway play important roles in nociceptive information processing. Our findings complement a recent study that identified the important spinal component of the neural circuit for the generation of nocifensive behaviors (Huang et al., 2019).

Interestingly, our results reveal that activation of the ipsilateral spinoparabrachial pathway rather than the contralateral pathway generates robust nocifensive behaviors. This is likely due to the difference in postsynaptic targets of the ipsilateral and contralateral spinoparabrachial pathways as demonstrated with several approaches in our study. Our results are in line with a previous study showing that the projection patterns in the ipsilateral and contralateral spinoparabrachial pathways are different (Bester et al., 1995), although Bester et al. showed contralateral side dominance, likely due to technical difference. The difference in postsynaptic targets of the ipsilateral and contralateral spinoparabrachial pathways partially explains why licking behaviors were observed only after activation of the ipsilateral pathway. Another possibility is that some spinal neurons send projections only to the ipsilateral or contralateral side (Li and Li, 2000). This remains to be determined but will be difficult to accomplish with current technology.

Another interesting observation is that photostimulation of the spinal fibers in the contralateral PBN evoked stronger vocalization than that of the ipsilateral PBN, indicating a stronger negative emotional component (Rodriguez et al., 2017). In line with this notion, photostimulation of the spinal fibers in the contralateral PBN also evoked stronger place aversion than that in the ipsilateral PBN. These results indicate that photostimulation of the spinal fibers in the contralateral PBN is likely to be more painful. However, in contrast to licking behaviors, vocalization and avoidance behavior induced by optogenetic activation of the spinal fibers in the PBN might not be mediated by the PBN. These behavioral responses evoked by photostimulation of the spinal fibers in the contralateral PBN could be mediated by coactivation of multiple ascending pathways, further supporting the idea that the activation of ascending fibers targeting different postsynaptic targets evokes diverse behaviors.

Neuronal Subtypes in the PBN Targeted by Spinal Projections

There are multiple subtypes of neurons in the PBN labeled by different molecular markers (Maeda et al., 2009). Previous studies reported that different subsets of neurons in the PBN are involved in distinct physiological processes (Campos et al., 2018; Nakamura and Morrison, 2008; Ryan et al., 2017). Our study identified that PBN *Tacr1*$^+$ neurons represent the major target of spinal projections in the PBN for processing nociceptive information. Our results showed that manipulation of the activity of PBN *Tacr1*$^+$ neurons modulated the nocifensive behavior bidirectionally. These behavioral results are consistent with the idea that *Tacr1*$^+$ neurons in the PBN play a key role in processing nociceptive information originating from the ascending spinoparabrachial pathway. This was further supported by fiber photometry data showing that PBN *Tacr1*$^+$ neurons were activated by noxious stimulation. Although PBN *Tacr1*$^+$ neurons represent the major target of spinal projections in the PBN, it is worth noting that not all *Tacr1*$^+$ neurons are targeted by spinal projection fibers, which could explain the behavioral difference following activation of *Tacr1*$^+$ neurons in the PBN and spinal projection fibers.

Our study complements a recent study showing that the *Tac1*$^+$ neurons in the PBNel gate the nocifensive behavior via a descending mechanism (Barik et al., 2018). Our study does not exclude the possible role of other subtypes of PBN neurons in pain. In fact, a recent study has shown that *Pdyn*$^+$ PBN neurons are important for pain affection (Chiang et al., 2020), although these neurons play a minor role in nocifensive behavior. Together with early studies that examined the functions of multiple subtypes of PBN neurons (Alhadeff et al., 2018; Carter et al., 2013; Chiang et al., 2019; Han et al., 2015; Mu et al., 2017; Qiu et al., 2016; Ryan et al., 2017), our results further emphasize the importance of dissecting the functional roles of different neuronal subtypes in the PBN.

The Spinal Cord/PBN/CeA Pathway

It has been long thought that the PBN relays nociceptive information from the spinal cord to the CeA (Jasmin et al., 1997; Richard et al., 2005). However, our results demonstrate that direct connections between PBN_{SC} and CeA neurons are limited. In line with previous studies (Jasmin et al., 1997), we found that PBN_{CeA} neurons were located in the PBNel, which is different from the location of PBN_{SC} neurons that were mostly located in the PBNsl. Although a recent study suggested that spinal projection neurons synapse with *CGRP*$^+$ neurons (Huang et al., 2019), a subpopulation of PBN_{CeA} neurons in the PBNel, this synaptic connection was not examined experimentally. In addition, we detected no functional synaptic connection between PBN_{SC} and CeA neurons, further supporting that PBN does not directly channel spinal nociceptive signals to CeA. Our tracing and electrophysiological results showed that PBN_{SC} neurons send few direct projections to CeA, which are inconsistent with the traditional notion that PBN_{SC} neurons can directly convey nociceptive signals to CeA. This discrepancy is likely due to the technical limitations of early studies.

Although there are limited direct connections between PBN_{SC} neurons and CeA neurons, PBN_{SC} neurons could send information to CeA indirectly. Our electrophysiological study showed a small percentage of functional connections between PBN_{SC} neurons and PBN_{CeA} neurons, indicating indirect connection between PBN_{SC} neurons and CeA neurons. Our result is in line with a recent study suggesting that the local circuit in the PBN is involved in relaying information from the spinal cord to the CeA (Chiang et al., 2020). Given that *CGRP*$^+$ neurons in the PBN, which represent a significant proportion of PBN_{CeA} neurons, are strongly activated by noxious stimuli (Campos et al., 2018), some other pathways could be involved in relaying somatosensory information to PBN_{CeA} neurons (Rodriguez et al., 2017).

The PBN Directly Relays Nociceptive Information from the Spinal Cord to the ILN

We have provided convincing evidence that nociceptive information conveyed by the spinoparabrachial pathway is directly relayed to the ILN. By labeling PBN_{SC} and PBN_{ILN} neurons in the same animals, we found that these two populations of neurons exhibit substantial colocalization. Consistently, by expressing EYFP in PBN_{SC} neurons, we observed dense EYFP$^+$ fibers in the ILN. Furthermore, using electrophysiological experiments, we confirmed that PBN_{SC} neurons form functional glutamatergic connections with neurons in the ILN.

In line with the anatomical results, we found that ILN neurons were activated by noxious stimulation, similar to PBN neurons. These data are consistent with previous studies indicating that the ILN is involved in pain processing (Harte et al., 2004; Munn et al., 2009; Thoden et al., 1979). Although the activation of ILN neurons in response to noxious stimuli could be partially mediated by sparse spinal projection (Huang et al., 2019), our data are more in line with the idea that the PBN directly channels the spinal nociceptive signal to the ILN via glutamatergic connections. This is supported by a previous study showing that the ILN receives inputs from the PBN (Bester et al., 1999) and that the PBN conveys nociceptive messages from the spinal cord to the ILN (Bourgeais et al., 2001). It is worth noting that PBN_{SC} neurons project to multiple brain areas besides the ILN. A recent study showed that different downstream pathways originating from the PBN were required for escape behaviors and nociception (Chiang et al., 2020). Thus, different projection could be involved in diverse processes of nociception. More studies are needed to further examine the functional role of different downstream pathways of PBN_{SC} neurons.

In summary, we have demonstrated the important role of the ipsilateral spinoparabrachial pathway in producing nocifensive behaviors and identified *Tacr1*$^+$ neurons as the key neuronal subtype in the PBN that is involved in this pathway. Our results reveal that the PBN does not directly relay nociceptive information from the spinal cord to the CeA but directly sends nociceptive information to the ILN instead. Thus, this study delineates an important circuit that conveys nociceptive information from the spinal cord to the brain.

STAR★METHODS

Detailed methods are provided in the online version of this paper and include the following:

- KEY RESOURCES TABLE
- RESOURCE AVAILABILITY
  - Lead Contact
  - Materials Availability
  - Data and Code Availability
- EXPERIMENTAL MODEL AND SUBJECT DETAILS
  - Mouse lines
- METHOD DETAILS
  - Stereotaxic injection
  - Surgery for viral injection into the spinal cord
  - Surgery for the viral injection and optical fiber or cannula implantation into the brain
  - Brain slice electrophysiology
  - Fiber photometry
  - Pain-related behaviors
  - Formalin test
  - Real-time place avoidance
  - Immunofluorescent staining
  - *In situ* hybridization
  - RNAscope
  - Imaging and analysis
- QUANTIFICATION AND STATISTICAL ANALYSIS

SUPPLEMENTAL INFORMATION

Supplemental Information can be found online at https://doi.org/10.1016/j.neuron.2020.06.017.

ACKNOWLEDGMENTS

We thank Yan-Jing Zhu, Xiao-Jun Chen, and Lei Yuan for technical support and all the members of the Yan-Gang Sun laboratory for helpful discussion. We thank Dr. Qian Hu and the optical imaging core facility for their assistance in imaging and data analysis. We thank Dr. Xiang Yu for providing the AAV2/8-hSyn-DIO-synaptophysin-tdTomato construct and Dr. Miao He for providing the H2B-GFP mice. This work is supported by the National Natural Science

Foundation of China (grants 61890952 and 31825013), the Shanghai Municipal Science and Technology Major Project (grant 2018SHZDZX05), and the Strategic Priority Research Program of the Chinese Academy of Sciences (grant XDB32010200). J.D. is supported by the National Postdoctoral Program for Innovative Talents of China (grant BX201800340), the Shanghai Post-doctoral Excellence Program (grant 2018032), and the SA-SIBS Scholarship Program.

AUTHOR CONTRIBUTIONS

Y.-G.S. and J.D. conceived the idea and designed the experiments. J.D., H.Z., Z.-X.S., J.-K.L., L.-H.W., and Q.L. performed the behavioral and histological experiments. J.D., H.Z., and W.-Z.C. performed fiber photometry experiments and analyzed the data. J.D. and D.M. performed slice recording experiments. J.D., Y.-C.W., and X.-H.X. performed vocalization experiments and analyzed the data. Y.-G.S. and J.D. wrote the manuscript.

DECLARATION OF INTERESTS

The authors declare no competing interests.

Received: January 24, 2019
Revised: March 26, 2020
Accepted: June 15, 2020
Published: July 9, 2020

REFERENCES

Alhadeff, A.L., Su, Z., Hernandez, E., Klima, M.L., Phillips, S.Z., Holland, R.A., Guo, C., Hantman, A.W., De Jonghe, B.C., and Betley, J.N. (2018). A neural circuit for the suppression of pain by a competing need state. Cell *173*, 140–152.

Al-Khater, K.M., and Todd, A.J. (2009). Collateral projections of neurons in laminae I, III, and IV of rat spinal cord to thalamus, periaqueductal gray matter, and lateral parabrachial area. J. Comp. Neurol. *515*, 629–646.

Armbruster, B.N., Li, X., Pausch, M.H., Herlitze, S., and Roth, B.L. (2007). Evolving the lock to fit the key to create a family of G protein-coupled receptors potently activated by an inert ligand. Proc. Natl. Acad. Sci. USA *104*, 5163–5168.

Barik, A., Thompson, J.H., Seltzer, M., Ghitani, N., and Chesler, A.T. (2018). A brainstem-spinal circuit controlling nocifensive behavior. Neuron *100*, 1–13.

Bernard, J.F., Bester, H., and Besson, J.M. (1996). Involvement of the spino-parabrachio -amygdaloid and -hypothalamic pathways in the autonomic and affective emotional aspects of pain. Prog. Brain Res. *107*, 243–255.

Bester, H., Menendez, L., Besson, J.M., and Bernard, J.F. (1995). Spino (trigemino) parabrachiohypothalamic pathway: electrophysiological evidence for an involvement in pain processes. J. Neurophysiol. *73*, 568–585.

Bester, H., Matsumoto, N., Besson, J.M., and Bernard, J.F. (1997). Further evidence for the involvement of the spinoparabrachial pathway in nociceptive processes: a c-Fos study in the rat. J. Comp. Neurol. *383*, 439–458.

Bester, H., Bourgeais, L., Villanueva, L., Besson, J.M., and Bernard, J.F. (1999). Differential projections to the intralaminar and gustatory thalamus from the parabrachial area: a PHA-L study in the rat. J. Comp. Neurol. *405*, 421–449.

Bester, H., Chapman, V., Besson, J.M., and Bernard, J.F. (2000). Physiological properties of the lamina I spinoparabrachial neurons in the rat. J. Neurophysiol. *83*, 2239–2259.

Bourgeais, L., Monconduit, L., Villanueva, L., and Bernard, J.F. (2001). Parabrachial internal lateral neurons convey nociceptive messages from the deep laminas of the dorsal horn to the intralaminar thalamus. J. Neurosci. *21*, 2159–2165.

Campos, C.A., Bowen, A.J., Roman, C.W., and Palmiter, R.D. (2018). Encoding of danger by parabrachial CGRP neurons. Nature *555*, 617–622.

Cao, H., Li, M.Y., Li, G., Li, S.J., Wen, B., Lu, Y., and Yu, X. (2020). Retinoid X receptor α regulates DHA-dependent spinogenesis and functional synapse formation in vivo. Cell Rep. *31*, 107649.

Carter, M.E., Soden, M.E., Zweifel, L.S., and Palmiter, R.D. (2013). Genetic identification of a neural circuit that suppresses appetite. Nature *503*, 111–114.

Cetin, A., Komai, S., Eliava, M., Seeburg, P.H., and Osten, P. (2006). Stereotaxic gene delivery in the rodent brain. Nat. Protoc. *1*, 3166–3173.

Chiang, M.C., Bowen, A., Schier, L.A., Tupone, D., Uddin, O., and Heinricher, M.M. (2019). Parabrachial Complex: A Hub for Pain and Aversion. J. Neurosci. *39*, 8225–8230.

Chiang, M.C., Nguyen, E.K., Canto-Bustos, M., Papale, A.E., Oswald, A.-M.M., and Ross, S.E. (2020). Divergent neural pathways emanating from the lateral parabrachial nucleus mediate distinct components of the pain response. Neuron *106*, 1–13.

Duan, B., Cheng, L., and Ma, Q. (2018). Spinal circuits transmitting mechanical pain and itch. Neurosci. Bull. *34*, 186–193.

Feil, K., and Herbert, H. (1995). Topographic organization of spinal and trigeminal somatosensory pathways to the rat parabrachial and Kölliker-Fuse nuclei. J. Comp. Neurol. *353*, 506–528.

Gao, Z.R., Chen, W.Z., Liu, M.Z., Chen, X.J., Wan, L., Zhang, X.Y., Yuan, L., Lin, J.K., Wang, M., Zhou, L., et al. (2019b). Tac1-expressing neurons in the periaqueductal gray facilitate the itch-scratching cycle via descending regulation. Neuron *101*, 45–59.

Gao, S.-C., Wei, Y.-C., Wang, S.-R., and Xu, X.-H. (2019a). Medial preoptic area modulates courtship ultrasonic vocalization in adult male mice. Neurosci. Bull. *35*, 697–708.

Gauriau, C., and Bernard, J.F. (2004). A comparative reappraisal of projections from the superficial laminae of the dorsal horn in the rat: the forebrain. J. Comp. Neurol. *468*, 24–56.

Gunaydin, L.A., Grosenick, L., Finkelstein, J.C., Kauvar, I.V., Fenno, L.E., Adhikari, A., Lammel, S., Mirzabekov, J.J., Airan, R.D., Zalocusky, K.A., et al. (2014). Natural neural projection dynamics underlying social behavior. Cell *157*, 1535–1551.

Han, S., Soleiman, M.T., Soden, M.E., Zweifel, L.S., and Palmiter, R.D. (2015). Elucidating an affective pain circuit that creates a threat memory. Cell *162*, 363–374.

Harte, S.E., Hoot, M.R., and Borszcz, G.S. (2004). Involvement of the intralaminar parafascicular nucleus in muscarinic-induced antinociception in rats. Brain Res. *1019*, 152–161.

He, M., Tucciarone, J., Lee, S., Nigro, M.J., Kim, Y., Levine, J.M., Kelly, S.M., Krugikov, I., Wu, P., Chen, Y., et al. (2016). Strategies and tools for combinatorial targeting of GABAergic neurons in mouse cerebral cortex. Neuron *91*, 1228–1243.

Huang, T., Lin, S.H., Malewicz, N.M., Zhang, Y., Zhang, Y., Goulding, M., LaMotte, R.H., and Ma, Q. (2019). Identifying the pathways required for coping behaviours associated with sustained pain. Nature *565*, 86–90.

Hylden, J.L., Anton, F., and Nahin, R.L. (1989). Spinal lamina I projection neurons in the rat: collateral innervation of parabrachial area and thalamus. Neuroscience *28*, 27–37.

Jansen, N.A., and Giesler, G.J., Jr. (2015). Response characteristics of pruriceptive and nociceptive trigeminoparabrachial tract neurons in the rat. J. Neurophysiol. *113*, 58–70.

Jasmin, L., Burkey, A.R., Card, J.P., and Basbaum, A.I. (1997). Transneuronal labeling of a nociceptive pathway, the spino-(trigemino-)parabrachio-amygdaloid, in the rat. J. Neurosci. *17*, 3751–3765.

Kamiyama, T., Kameda, H., Murabe, N., Fukuda, S., Yoshioka, N., Mizukami, H., Ozawa, K., and Sakurai, M. (2015). Corticospinal tract development and spinal cord innervation differ between cervical and lumbar targets. J. Neurosci. *35*, 1181–1191.

Krout, K.E., and Loewy, A.D. (2000). Parabrachial nucleus projections to midline and intralaminar thalamic nuclei of the rat. J. Comp. Neurol. *428*, 475–494.

Li, H., and Li, Y.Q. (2000). Collateral projection of substance P receptor expressing neurons in the medullary dorsal horn to bilateral parabrachial nuclei of the rat. Brain Res. Bull. *53*, 163–169.

Liu, Y., Broman, J., Zhang, M., and Edvinsson, L. (2009). Brainstem and thalamic projections from a craniovascular sensory nervous centre in the rostral cervical spinal dorsal horn of rats. Cephalalgia *29*, 935–948.

Maeda, N., Onimura, M., Ohmoto, M., Inui, T., Yamamoto, T., Matsumoto, I., and Abe, K. (2009). Spatial differences in molecular characteristics of the pontine parabrachial nucleus. Brain Res. *1296*, 24–34.

Menendez, L., Bester, H., Besson, J.M., and Bernard, J.F. (1996). Parabrachial area: electrophysiological evidence for an involvement in cold nociception. J. Neurophysiol. *75*, 2099–2116.

Missig, G., Mei, L., Vizzard, M.A., Braas, K.M., Waschek, J.A., Ressler, K.J., Hammack, S.E., and May, V. (2017). Parabrachial pituitary adenylate cyclase-activating polypeptide activation of amygdala endosomal extracellular signal-regulated kinase signaling regulates the emotional component of pain. Biol. Psychiatry *81*, 671–682.

Mu, D., Deng, J., Liu, K.F., Wu, Z.Y., Shi, Y.F., Guo, W.M., Mao, Q.Q., Liu, X.J., Li, H., and Sun, Y.G. (2017). A central neural circuit for itch sensation. Science *357*, 695–699.

Munn, E.M., Harte, S.E., Lagman, A., and Borszcz, G.S. (2009). Contribution of the periaqueductal gray to the suppression of pain affect produced by administration of morphine into the intralaminar thalamus of rat. J. Pain *10*, 426–435.

Nakamura, K., and Morrison, S.F. (2008). A thermosensory pathway that controls body temperature. Nat. Neurosci. *11*, 62–71.

Palmiter, R.D. (2018). The parabrachial nucleus: CGRP neurons function as a general alarm. Trends Neurosci. *41*, 280–293.

Polgár, E., Wright, L.L., and Todd, A.J. (2010). A quantitative study of brainstem projections from lamina I neurons in the cervical and lumbar enlargement of the rat. Brain Res. *1308*, 58–67.

Qiu, M.H., Chen, M.C., Fuller, P.M., and Lu, J. (2016). Stimulation of the pontine parabrachial nucleus promotes wakefulness via extra-thalamic forebrain circuit nodes. Curr. Biol. *26*, 2301–2312.

Richard, S., Engblom, D., Paues, J., Mackerlova, L., and Blomqvist, A. (2005). Activation of the parabrachio-amygdaloid pathway by immune challenge or spinal nociceptive input: a quantitative study in the rat using Fos immunohistochemistry and retrograde tract tracing. J. Comp. Neurol. *481*, 210–219.

Rinaldi, P.C., Young, R.F., Albe-Fessard, D., and Chodakiewitz, J. (1991). Spontaneous neuronal hyperactivity in the medial and intralaminar thalamic nuclei of patients with deafferentation pain. J. Neurosurg. *74*, 415–421.

Rodriguez, E., Sakurai, K., Xu, J., Chen, Y., Toda, K., Zhao, S., Han, B.X., Ryu, D., Yin, H., Liedtke, W., and Wang, F. (2017). A craniofacial-specific monosynaptic circuit enables heightened affective pain. Nat. Neurosci. *20*, 1734–1743.

Roeder, Z., Chen, Q., Davis, S., Carlson, J.D., Tupone, D., and Heinricher, M.M. (2016). Parabrachial complex links pain transmission to descending pain modulation. Pain *157*, 2697–2708.

Ryan, P.J., Ross, S.I., Campos, C.A., Derkach, V.A., and Palmiter, R.D. (2017). Oxytocin-receptor-expressing neurons in the parabrachial nucleus regulate fluid intake. Nat. Neurosci. *20*, 1722–1733.

Spike, R.C., Puskár, Z., Andrew, D., and Todd, A.J. (2003). A quantitative and morphological study of projection neurons in lamina I of the rat lumbar spinal cord. Eur. J. Neurosci. *18*, 2433–2448.

Sun, Y.G., Rupprecht, V., Zhou, L., Dasgupta, R., Seibt, F., and Beierlein, M. (2016). mGluR1 and mGluR5 synergistically control cholinergic synaptic transmission in the thalamic reticular nucleus. J. Neurosci. *36*, 7886–7896.

Tervo, D.G., Hwang, B.Y., Viswanathan, S., Gaj, T., Lavzin, M., Ritola, K.D., Lindo, S., Michael, S., Kuleshova, E., Ojala, D., et al. (2016). A designer AAV variant permits efficient retrograde access to projection neurons. Neuron *92*, 372–382.

Thoden, U., Doerr, M., Dieckmann, G., and Krainick, J.U. (1979). Medial thalamic permanent electrodes for pain control in man: an electrophysiological and clinical study. Electroencephalogr. Clin. Neurophysiol. *47*, 582–591.

Todd, A.J. (2010). Neuronal circuitry for pain processing in the dorsal horn. Nat. Rev. Neurosci. *11*, 823–836.

Veinante, P., Yalcin, I., and Barrot, M. (2013). The amygdala between sensation and affect: a role in pain. J. Mol. Psychiatry *1*, 9.

Williams, M.C., and Ivanusic, J.J. (2008). Evidence for the involvement of the spinoparabrachial pathway, but not the spinothalamic tract or post-synaptic dorsal column, in acute bone nociception. Neurosci. Lett. *443*, 246–250.

Xu, X., Coats, J.K., Yang, C.F., Wang, A., Ahmed, O.M., Alvarado, M., Izumi, T., and Shah, N.M. (2012). Modular genetic control of sexually dimorphic behaviors. Cell *148*, 596–607.

Zingg, B., Chou, X.L., Zhang, Z.G., Mesik, L., Liang, F., Tao, H.W., and Zhang, L.I. (2017). AAV-mediated anterograde transsynaptic tagging: mapping corticocollicular input-defined neural pathways for defense behaviors. Neuron *93*, 33–47.

STAR★METHODS

KEY RESOURCES TABLE

REAGENT or RESOURCE	SOURCE	IDENTIFIER
Antibodies		
Rabbit anti-GFP	Life Technology	Cat#A11122; RRID: AB_221569
Mouse anti-GFP	Life Technology	Cat#A11120; RRID: AB_221568
Rabbit anti-DsRed	Clontech	Cat#632496; RRID: AB_10013483
Donkey anti-rabbit IgG-Alexa 488	Jackson ImmunoResearch Laboratories	Cat#711-545-152; RRID: AB_2313584
Donkey anti-rabbit IgG-Cy3	Jackson ImmunoResearch Laboratories	Cat#711-165-152; RRID: AB_2307443
Donkey anti-mouse IgG-Alexa 488	Jackson ImmunoResearch Laboratories	Cat#715-545-150; RRID: AB_2340846
Bacterial and Virus Strains		
AAV2/9-hSyn-hChR2(H134R)-mCherry	Taitool	Cat#S0165
AAV2/8-hSyn-hM4Di-mCherry	Armbruster et al., 2007	Addgene: Cat#50475; RRID: Addgene_50475
AAV2/9-hSyn-EGFP	Taitool	Cat#S0237
AAV2/8-hSyn-DIO-synaptophysin-tdTomato	Taitool	Cat#XT140
AAV2/1-CMV-bGlobin-Cre-EGFP	Taitool	Cat#S0231
AAV2/1-hSyn-Flpo	Taitool	Cat#S0271
AAV2/9-hSyn-GCaMP6s	Taitool	Cat#S0225
AAV2/9-CAG-DIO-taCasp3-TEVp	Taitool	Cat#S0236
AAV2/9-EF1α-DIO-EYFP	Taitool	Cat#S0196
AAV2/5-hSyn-DIO-hM4Di-mCherry	UNC Vector Core	N/A
AAV2/9-EF1α-fDIO-EYFP	Taitool	Cat#S0253
AAV2/9-EF1α-fDIO-hM4Di-mCherry	Taitool	Cat#S0336
AAV2/8-EF1α-fDIO-hM3Dq-mCherry	Taitool	Cat#S0337
AAV2/9-EF1α-fDIO-mCherry	Taitool	Cat#S0553
AAV2/9-EF1α-fDIO-GCaMP6s	Taitool	Cat#S0352
rAAV2/2-retro-CMV-bGlobin-Cre-EGFP	Taitool	Cat#Retro-S0231
AAV2/9-EF1α-DIO-hChR2(H134R)-mCherry	Taitool	Cat#S0170
Chemicals, Peptides, and Recombinant Proteins		
Clozapine-n-oxide	Sigma	Cat#C0832
Red-Beads	Lumaflour	Cat#78R170
Green-Beads	Lumaflour	Cat#78G180
CTB-555	Invitrogen	Cat#C34776
Streptavidin, Alexa Fluor 488 conjugate	Invitrogen	Cat#11223
Streptavidin, Alexa Fluor 633 conjugate	Invitrogen	Cat#21375
NBQX	Tocris	Cat#1044
Picrotoxin	Tocris	Cat#1128
CPP	Tocris	Cat#0247
Poly-L-lysine	Sigma	Cat#P4707
Experimental Models: Organisms/Strains		
Mouse: C57BL/6N	SLAC laboratory	N/A
Mouse: Vglut2-Cre	The Jackson Laboratory	JAX016963
Mouse: SST-Cre	The Jackson Laboratory	JAX013044

(*Continued on next page*)

Continued

REAGENT or RESOURCE	SOURCE	IDENTIFIER
Mouse: Pdyn-Cre	The Jackson Laboratory	JAX 027958
Mouse: Ai9	The Jackson Laboratory	JAX 007905
Mouse: H2B-GFP	He et al., 2016	N/A
Mouse: Tacr1-flpo	This paper	N/A
Software and Algorithms		
GraphPad Prism 5	GraphPad	https://www.graphpad.com/scientific-software/prism/
Fiji (ImageJ)	NIH	https://fiji.sc/
F-scope	BiolinkOptics	http://www.biolinkoptics.com/
MATLAB	MathWorks	https://www.mathworks.com
Scorevideo	Xu et al., 2012	https://github.com/U8NWXD/scorevideo_lib
LabState	AniLab	N/A
Other		
Master-8	A.M.P.I	N/A
F-scope-G-2	BiolinkOptics	N/A
Optical fibers	AniLab	N/A

RESOURCE AVAILABILITY

Lead Contact

Further information and requests for resources and reagents should be directed to and will be fulfilled by the Lead Contact, Yan-Gang Sun (yangang.sun@ion.ac.cn).

Materials Availability

Mouse lines generated in this study can be requested by direct connect with the Lead Contact.

Data and Code Availability

All relevant data and code for this study can be made available by the Lead Contact upon reasonable request. The code supporting the current study has been deposited in public repository (https://github.com/Juan-DENG/code_SC_PBN).

EXPERIMENTAL MODEL AND SUBJECT DETAILS

Mouse lines

Male C57BL/6N, *Vglut2-Cre*, *Sst-Cre*, *Pdyn-Cre*, Ai9, H2B-GFP and *Tacr1-flpo* mice at the age of 6-10 weeks old were used for experiments. C57BL/6N mice were purchased from SLAC laboratory (Shanghai). *Vglut2-Cre* (JAX016963), *Sst-Cre* (JAX013044), *Pdyn-Cre* (JAX027958) and Ai9 (JAX007905) mice were initially acquired from Jackson laboratory, H2B-GFP mice were acquired from Miao He's lab at Fudan university (He et al., 2016). The *Tacr1-flpo* mouse line was generated using the CRISPR/Cas9 technique, in which the 2A-flpo was inserted before the stop codon of the last exon of the *Tacr1* gene. All mice were raised on a 12-hr light/dark cycle (light on at 7:00 am) with *ad libitum* food and water. All procedures were approved by the Animal Care and Use Committee of the Center for Excellence in Brain Science & Intelligence Technology, Chinese Academy of Sciences, Shanghai, China.

METHOD DETAILS

Stereotaxic injection

Mice were anesthetized with pentobarbital sodium (100 mg/kg, Mymtechnologies) and mounted in a stereotaxic apparatus (Stoelting Co., USA). Body temperature of mice was maintained with a heating pad (40-90-8D, FHC). Ophthalmic ointment was applied to eyes before the skull was exposed by midline scalp incision, then a small craniotomy (~1.5 mm diameter) was performed using a hand-held drill over the target site. Retro-beads (Red-beads or Green-beads, IX, Lumafluor), CTB-555 (Invitrogen) or viruses were injected into target brain areas at the rate of ~50 nL/min using an air pressure system [glass pipette was connected (tip diameter: 10-30 μm, prepared with pipette puller) to the Picospritzer III (Parker), controlled by Master-8 (A.M.P.I.)], or the oil pressure system [glass pipette

was filled with the mineral oil and connected to the oil pump (Narishige Scientific Instrument Lab), virus was filled into the pipette without air bubble]. After completion of the injection, the glass pipette was left in place for 5-10 min and withdrew slowly to avoid back-flow of virus or tracers to the surface. After that, we sutured the skin and put animals on a heating blanket before returning them to their home cages (Cetin et al., 2006).

Surgery for viral injection into the spinal cord

For intra-spinal cord viral injection, vertebrae of the mouse were exposed at L4-L6 and fixed on the stereotaxic frame. After removing tissues above the spinal cord, the dura was incised to expose the spinal cord (Kamiyama et al., 2015).

To label the spinoparabrachial pathway or record the postsynaptic currents in PBN neurons, AAV2/9-hSyn-hChR2(H134R)-mCherry (titer: 4.22×10^{12} v.g./mL, Taitool) virus was injected into the superficial dorsal spinal cord of the right side.

To manipulate the activity of the spinoparabrachial pathway, AAV2/9-hSyn-hChR2(H134R)-mCherry (titer: 4.22×10^{12} v.g./mL, Taitool) or AAV2/8-hSyn-hM4Di-mCherry (titer: 5.5×10^{12} v.g./mL, Addgene) virus was injected into the right superficial dorsal spinal cord, except for the activation of spinoparabrachial pathway arising from left spinal cord, in which virus was injected into the left side of superficial dorsal spinal cord. AAV2/9-hSyn-EGFP (titer: 4.4×10^{12} v.g./mL, Taitool) virus was injected as a control.

To label axon terminals of spinal projection neurons, AAV2/8-hSyn-DIO-synaptophysin-tdTomato virus (titer: 1.71×10^{13} v.g./mL, Taitool) was injected into the right superficial dorsal spinal cord of *Vglut2-Cre* mice.

To label PBN_{SC} neurons, AAV2/1-CMV-bGlobin-Cre-EGFP (titer: 1.39×10^{13} v.g./mL, Taitool) or AAV2/1-hSyn-Flpo (titer: 1.75×10^{13} v.g./mL, Taitool) virus was injected into the right superficial dorsal spinal cord of Ai9 or H2B-GFP mice.

AAV2/1-CMV-bGlobin-Cre-EGFP (titer: 1.39×10^{13} v.g./mL, Taitool) virus was injected into right superficial dorsal spinal cord of wild-type mice for the manipulation of PBN_{SC} neurons and the activation of axon terminals of PBN_{SC} neurons in CeA and ILN.

All viruses were injected into the spinal cord with 2-4 injection sites (interspaced by 400 μm, 400-600 nL/site), except for AAV2/1-CMV-bGlobin-Cre-EGFP and AAV2/1-hSyn-Flpo viruses, which were injected with only two injection sites (interspaced by 800 μm, 200 nL/site). Micropipette was inserted into the dorsal spinal cord at an angle (50-60 degrees) to target the superficial layers.

Surgery for the viral injection and optical fiber or cannula implantation into the brain

Injection sites for PBN, CeA and ILN were bregma: −5.4 mm, lateral: ± 1.2 mm, depth: −3.35 mm; bregma: −1.3 mm, lateral: ± 2.7 mm, depth: −4.6 mm; bregma: −1.68 mm, lateral: 0 mm, depth: −3.7 mm, respectively. All viruses were injected with a volume of 200-400 nL/site.

To test the neuronal activity of PBN neurons in response to various stimulation, AAV2/9-hSyn-GCaMP6s virus (titer: 3.36×10^{12} v.g./mL, Taitool) was injected into right PBN and optical fibers (AniLab) were implanted above the injection site, optical fibers were attached to the skull with dental cement (Mu et al., 2017). AAV2/9-hSyn-EGFP (titer: 4.4×10^{12} v.g./mL, Taitool) virus was injected as a control.

For activating the spinoparabrachial pathway, two weeks after viral injection into the spinal cord, optical fibers (AniLab) were implanted above the left and right PBN (bregma: −5.4 mm, lateral: ± 1.9 mm, depth: −2.7 mm at an angle of 15 degrees).

For inhibiting the spinoparabrachial pathway, two weeks after viral injection into the spinal cord, cannula (0.41 mm in diameter, Reward) were implanted above the left or right PBN (bregma: −5.3 mm, lateral: ± 1.15 mm, depth: 2.75 mm), cannula were attached to the skull with dental cement.

To ablate *Vglut2*$^+$, *Sst*$^+$ or *Pdyn*$^+$ neurons in PBN, AAV2/9-CAG-DIO-taCasp3-TEVp (titer: 5×10^{12} v.g./mL, Taitool) virus was injected into the right PBN, except for the ablation of contralateral PBN, which received virus injection in the left PBN. AAV2/9-EF1α-DIO-EYFP virus (titer: 5.75×10^{12} v.g./mL, Taitool) was injected as a control.

For manipulating the neuronal activity of PBN_{SC} neurons with DREADDs, one week after the injection of AAV2/1-CMV-bGlobin-Cre-EGFP virus (titer: 1.39×10^{13} v.g./mL, Taitool) into the right spinal cord, AAV2/5-hSyn-DIO-hM4Di-mCherry (titer: 5.1×10^{12} v.g./mL, UNC) or AAV2/9-EF1α-DIO-EYFP (titer: 5.75×10^{12} v.g./mL, Taitool) virus was injected into the right or left PBN.

To test the specificity and efficiency of *Tacr1-flpo* mice, AAV2/9-EF1α-fDIO-EYFP (titer: 3×10^{12} v.g./mL, Taitool) virus was injected into the right PBN of *Tacr1-flpo* mice, which were used for histological verification.

To manipulate the activity of *Tacr1*$^+$ PBN neurons, AAV2/9-EF1α-fDIO-hM4Di-mCherry (titer: 4.3×10^{12} v.g./mL, Taitool) or AAV2/8-EF1α-fDIO-hM3Dq-mCherry (titer: 3.9×10^{12} v.g./mL, Taitool) virus was injected into the right PBN of *Tacr1-flpo* mice. AAV2/9-EF1α-fDIO-mCherry (titer: 4×10^{12} v.g./mL, Taitool) or AAV2/9-EF1α-fDIO-EYFP (titer: 3×10^{12} v.g./mL, Taitool) virus was injected as a control.

To examine the neuronal activity of *Tacr1*$^+$ PBN neurons in response to various stimuli, AAV2/9-EF1α-fDIO-GCaMP6s (titer: 8.4×10^{12} v.g./mL, Taitool) virus was injected into the right PBN of *Tacr1-flpo* mice, followed by implantation of optical fibers above the injection site.

To simultaneously label CeA or ILN projecting neurons and PBN_{SC} neurons in PBN, Red-beads (400 nL), CTB-555 (400 nL) were injected into CeA or ILN of H2B-GFP mice that injected with AAV2/1-hSyn-Flpo virus in the right spinal cord.

rAAV2/2-retro-CMV-bGlobin-Cre-EGFP virus (titer: 7.5×10^{12} v.g./mL, Taitool) was injected into CeA and AAV2/9-hSyn-DIO-mCherry virus (titer: 3×10^{12} v.g./mL, Taitool) was injected into PBN to label CeA-projecting PBN neurons.

For the tracing experiment, AAV2/9-EF1α-DIO-EYFP virus (titer: 5.75×10^{12} v.g./mL, Taitool) was injected into the right PBN of mice that were injected with AAV2/1-CMV-bGlobin-Cre-EGFP virus (titer: 1.39×10^{13} v.g./mL, Taitool) into the right spinal cord.

To test connections between PBN_{SC} neurons and neurons in ILN or CeA, AAV2/9-EF1α-DIO-hChR2(H134R)-mCherry virus (titer: 4×10^{12} v.g./mL, Taitool) was injected into the right PBN of mice that were injected with AAV2/1-CMV-bGlobin-Cre-EGFP virus (titer: 1.39×10^{13} v.g./mL, Taitool) into the right spinal cord.

To define connections between PBN_{SC} neurons and CeA-projecting neurons in PBN, AAV2/9-EF1α-DIO-hChR2(H134R)-mCherry virus (titer: 4×10^{12} v.g./mL, Taitool) was injected into the right PBN and Green-beads (400 nL) was injected into CeA of mice that were injected with AAV2/1-CMV-bGlobin-Cre-EGFP virus (titer: 1.39×10^{13} v.g./mL, Taitool) into the right spinal cord.

To examine the neuronal activity of ILN neurons in response to various stimuli, AAV2/9-hSyn-GCaMP6s virus (titer: 3.36×10^{12} v.g./mL, Taitool) was injected into ILN, followed by implantation of optical fibers above the injection site.

Brain slice electrophysiology

Slice electrophysiology were performed as described previously (Sun et al., 2016). Mice were anesthetized with isoflurane (Lunan Pharmaceutical) and perfused with the ice-cold cutting solution containing (in mM) sucrose 213, KCl 2.5, NaH_2PO_4 1.25, $MgSO_4$ 10, $CaCl_2$ 0.5, $NaHCO_3$ 26, and glucose 11 (300-305 mOsm). The brain was then rapidly dissected, and coronal slices (220-300 μm) were prepared in the ice-cold cutting solution, using a vibratome (Leica VT1200S) at the speed of 0.12 mm/s and a blade vibration amplitude of 0.8 mm. Slices were transferred to the holding chamber and incubated in the artificial cerebral spinal fluid (ACSF, 34°C) containing (in mM) NaCl 126, KCl 2.5, NaH_2PO_4 1.25, $MgCl_2$ 2, $CaCl_2$ 2, $NaHCO_3$ 26, and glucose 10 (300-305 mOsm) to recover for 40 min, then kept at room temperature prior to recording. Both the cutting solution and ACSF were continuously bubbled with 95% O_2/5% CO_2.

Slices were placed on the Poly-L-lysine (Sigma, St. Louis, MO) coated coverslips, and submerged in the recording chamber (Warner Instruments, Hamden, CT). The chamber was perfused with ACSF at 3-4 mL/min using a pump (BT100-2J, LongerPump). Whole-cell patch-clamp recordings were made from target neurons under IR-DIC visualization and a CCD camera (IR-1000E, DAGE-MTI) using an Olympus BX51WI microscope (Olympus Optical, Tokyo, Japan). The cesium-based internal solution contained (in mM) $CsMeSO_3$ 130, $MgCl_2$ 1, $CaCl_2$ 1, HEPES 10, QX-314 2, EGTA 11, Mg-ATP 2, Na-GTP 0.3 (pH 7.3, 295 mOsm) was used for voltage-clamp recording. The potassium-based internal solution contained (in mM) K-gluconate 130, $MgCl_2$ 1, $CaCl_2$ 1, KCl 1, HEPES 10, EGTA 11, Mg-ATP 2, Na-GTP 0.3 (pH 7.3, 290 mOsm) was used for current-clamp recording. Blue LED (UHP-Mic-LED-475, Prizmatix, Israel) or laser (473 nm, CrystaLaser) was used to activate $ChR2^+$ fibers or neurons. NBQX, CPP and picrotoxin were purchased from Tocris. All other chemicals are obtained from Sigma, unless otherwise noted.

Fiber photometry

For measuring the neuronal activity of PBN or ILN, we recorded Ca^{2+} transients with F-scope-G-2 (BiolinkOptics), the onset and offset points of the stimulus were recorded with a digital camera or labeled with Master 8 (A.M.P.I.) triggered analog signals simultaneously (Gao et al., 2019b).

Mice were anesthetized by injecting pentobarbital sodium (60-80 mg/kg). To test the neuronal activity in response to mechanical stimulation, mice received pinches (5 s) using the forceps on the tail and four paws, or light mechanical stimuli (3 s) on the tail using a brush. To examine neural activity in response to thermal stimulation, tails of mice were immersed into a temperature-controlled water bath ranging from 40°C to 52°C (20 s for 40°C and 46°C, 10 s for 52°C). For testing the neuronal activity in response to noxious cold stimulation, calcium fluorescent signal was recorded before and after placing a piece of dry-ice on the left hind paw of mice (20 s for wild-type mice and 5 s for *Tacr1-flpo* mice). All these tests were performed on anesthetized mice, and all mice were perfused immediately after the cold pain test.

For the foot shock stimulation, electric shock (0.3 mA) was delivered to mice for 2 s. In hot plate test, mice were introduced into a pre-heated aluminum plate (20 s for 40°C and 48°C, 10 s for 56°C) enclosed within a transparent Plexiglas chamber (Campos et al., 2018). These two tests were performed in awake mice.

At the end of the experiment, all animals were perfused. Only data from animals with correct optical fiber implantation sites and virus expression were included for analysis. Onset and offset points of the stimulation were determined by analyzing the video frame-by-frame or retrieving analog signals with the MATLAB program. After subtracting noise signals of the fiber photometry recording system, we smoothed the data with a moving average filter (20 ms-span). The values of Ca^{2+} transients change (ΔF/F) from −10 s to 30 s (0 s, stimuli onset) were derived by calculating (F-F0)/F0 for each trial, where F0 was defined as the mean Ca^{2+} transients from −10 s to −5 s in the hot plate test and −5 s to 0 s in other tests.

Pain-related behaviors

For optogenetic evoked pain-related behaviors, mice were introduced to a plastic box (width: 10 cm, length: 10 cm, height: 15 cm) and were videotaped from the bottom. A custom MATLAB program was started to control the Master 8 (A.M.P.I.), which sent a trigger pulse (10 ms) to light the LED (recorded by the camera) and signals to deliver photostimulation (473 nm, 5 ms) for 30 s with different frequencies (40 Hz, 20 Hz or 10 Hz) and intensities (10 mW, 5 mW or 1 mW) separated by 60-90 s intervals for 4 trials. The trigger signal to LED was used to synchronize the light stimulation with the video. During the videotaping, sounds at the frequency range of 0 KHz∼125 KHz were recorded with a microphone, and the signals were amplified (UltraSoundGate, Avisoft Bioacoustics) and digitized at 250 KHz and 16 bits. At the beginning of the record, a short noise was made manually under the video field to synchronize the voice with the video. For optogenetics-induced pain-related behaviors, licking and flinching behaviors were scored manually with the

scorevideo code (Xu et al., 2012). For the light-evoked vocalization, the stored waveforms were converted to spectrogram using the MATLAB-based program (128 samples/block form, time resolution of 0.2 ms and frequency resolution of 0.98 KHz) and extracted by 3 times larger than the standard deviation of baseline (Gao et al., 2019a). The extracted vocalization or scored behaviors were aligned to the blue light stimulation to calculate the duration of light-evoked behaviors.

For the pharmacogenetics-induced pain-related behaviors, mice were introduced into a Plexiglas box (width: 10 cm, length: 10 cm, height: 15 cm) individually after the injection of CNO (1 mg/kg or 2 mg/kg, i.p., Sigma) or saline. Thirty min after the CNO injection, behaviors of mice were recorded for 1 hr. Pain-related licking and flinching behaviors were analyzed manually with the scorevideo code.

Formalin test

In formalin test, formalin (5%, 10 μL/mouse) was injected into the right hind paw of mice. After the formalin injection, mice were immediately introduced into a plexiglas box (width: 10 cm, length: 10 cm, height: 15 cm) individually with their behaviors recorded for 1 hr. For pharmacogenetic inactivation of spinal projection fibers in PBN, formalin test was performed 30 min after the infusion of CNO (0.5 μg/site, Sigma) into the ipsilateral or contralateral PBN. For pharmacogenetic inhibition of PBN_{SC} neurons and *Tacr1*$^{+}$ PBN neurons, formalin test was performed 30 min after the injection of CNO (1 mg/kg, i.p., Sigma). For mice with different subsets of PBN neurons ablated, formalin test was performed after habituating animals in the recording box for 15 min. Time exhibiting pain-related licking and flinching behaviors for animals were scored manually with the scorevideo code (Xu et al., 2012). All videos were analyzed by trained investigators blinded to the experimental treatment of the animals.

Real-time place avoidance

Two weeks after the implantation of optical fibers in PBN, mice were individually introduced into a two-chamber box (one chamber with black walls and the other chamber with white walls) and recorded for 30 min (Rodriguez et al., 2017). Briefly, after a 15 min baseline recording period, light stimulation (20 Hz, 5 ms pulse-width, 10 mW) was delivered on the left or right PBN whenever the mice entered or stayed in the black chamber, and light was turned off when the mice moved to the other chamber. The avoidance score was defined as the duration of time spent in the black chamber during the light-on period minus that of the baseline period. For this test, every mouse was tested for only once to avoid the effect of the memory.

Immunofluorescent staining

Mice were anesthetized with pentobarbital sodium (100 mg/kg, Mymtechnologies), and perfused with saline followed by 4% paraformaldehyde (PFA, Sigma). After the perfusion, the brain and/or spinal cord were dissected, and post-fixed in 4% PFA for overnight at 4°C, followed by cryoprotecting in 30% sucrose. Free-floating sections (30 μm) prepared with the cryostat (Leica CM 1950) were used for immunohistochemical staining, except for spinal cord and brains that implanted with optical fibers or cannula, which were mounted on slides immediately after sectioning. Tissue sections were blocked for 30 min at room temperature in PBST (0.3% Triton X-100) with 3% normal donkey serum, followed by incubating with primary antibodies at 4°C for overnight and secondary antibodies at room temperature for 2 hr. Primary antibodies used in immunohistochemistry (IHC) were rabbit anti-DsRed (Clontech, 632496), rabbit anti-GFP (Life Technology, A11122), mouse anti-GFP (Life Technology, A11120). All primary antibodies were used at a concentration of 1:500 for floating sections and 1:200 for other tissues. Secondary antibodies were donkey anti-rabbit IgG-Alexa 488 (Jackson ImmunoResearch Laboratories, 711-545-152), donkey anti-mouse IgG-Alexa 488 (Jackson ImmunoResearch Laboratories, 715-545-150), donkey anti-rabbit IgG-Cy3 (Jackson ImmunoResearch Laboratories, 711-165-152). All secondary antibodies were used at a concentration of 1:400 for floating sections and 1:200 for other tissues. DyLight 633 (1:500, Invitrogen, S21375), 488 conjugated streptavidin protein (1:500, Invitrogen, S11223) was used to detect the electrophysiological recorded neurons.

In situ hybridization

To determine the overlapping of different PBN neuron types and PBNsc neurons, *in situ* hybridization and immunofluorescent double-staining were performed. Brains of H2B-GFP mice that were injected with AAV2/1-hSyn-Flpo virus in the spinal cord were sectioned at 40 μm with a cryostat (Leica CM 1950), sections were collected into the cold DepC-PBS. Floating sections were washed once (5 min) in DepC-PBS and twice (5 min for each time) in DepC-PTW (PBS-Tween, PBS with 0.1% Tween-20). Then, the brain sections were washed in the Triton X-100 (0.5%) contained 2 × SSC for 30 min, followed by washing in DepC-PTW. After acetylating in triethanolamine (0.1 M, pH 8.0) with 0.25% acetic anhydride for 10 min, the sections were pre-hybridized with the pre-hybridization buffer (hereafter referred to as pre-hyb) at 65°C for 2 hr and hybridized with the *CGRP*, *Pdyn*, *Sst* or *Tacr1* probe (0.5 μg/mL) at 65°C for 16-18 hr. After that, the sections were rinsed in the pre-hyb buffer for 30 min, followed by rinsing in the pre-hyb/TBST (TBS-Tween, TBS with 0.1% Tween-20) buffer for 30 min. Next, the sections were washed with TBST for twice and TAE for three times (5 min for each time). After that, sections were transferred to wells made with the agarose gel (2% in TAE), and electrophoresis (60 V) was conducted to the sections for 2 hr. The sections were then washed twice in TBST buffer, and incubated with sheep anti-DIG-AP (1:2000, Roche) and rabbit anti-GFP (1:500, Life Technology) antibody in 0.5% blocking reagent (Roche, 11096176001) at 4°C for overnight. On the second day, sections were washed for three times in the TBST (30 min for each time), then balanced in the AP buffer [containing 50 mM $MgCl_2$, 100 mM NaCl, 0.1% Tween-20, 100 mM Tris, Levamisole (2 mM/L, Sigma, L9756), pH 9.5] for two times (30 min for each time) and visualized with BCIP (50 mg/mL, Roche) and NBT (75 mg/mL, Roche) for 3-36 hr. After the hybridization staining,

sections were incubated with the secondary antibody (donkey anti-rabbit IgG-Alexa 488, 1:250, Jackson ImmunoResearch Laboratories) at room temperature for 2 hr, washed with PBS and counterstained with DAPI (1:10000). After that, sections were mounted on slides.

To test the ablation efficiency of AAV2/9-CAG-DIO-taCasp3-TEVp virus, *in situ* hybridization were performed to define the expression of *Vglut2*, *Sst* and *Cre* in PBN. Slides were heated on the slide heater (60°C) for 1.5 hr, fixed in DepC-PFA (4% paraformaldehyde in DepC-PBS) for 20 min and washed in DepC-PBS for 5 min. Then, slides were treated with Proteinase K (10 μg/mL) in PK buffer [1 M Tris-HCl (pH 7.5), 0.5 M EDTA] for 12 min, washed in DepC-PBS for 5 min and fixed in DepC-PFA for 20 min. After that, slides were rinsed once in DepC-ddH_2O, acetylated in triethanolamine with 0.25% acetic anhydride for 8 min, and washed in DepC-PBS for 5 min. After that, slides were pre-hybridized in the pre-hyb buffer at 60°C for 4 hr, and hybridized with the *Vglut2*, *Sst* or *Cre* probe (1 μg/mL) for 12-16 hr at 60°C. On the second day, series of washing steps were performed using several pre-warmed buffers: 1 × SSC at 60°C for 10 min, 1.5 × SSC at 60°C for 10 min, 2 × SSC at 37°C for twice (20 min for each time). Then slides were treated with RNase A (3 μg/mL) in 2 × SSC at 37°C for 30 min, washed in 2 × SSC at room temperature for 10 min, 0.2 × SSC at 60°C for twice (30 min for each time), 0.2 × SSC at room temperature for 15 min and PBST at room temperature for 15 min. Slides were then incubated in heat-inactivated sheep serum (20%) contained PBST for 1-5 hr, and incubated with anti-DIG antibody (1:2000 in PBST with 20% sheep serum) at 4°C for overnight. On the next day, after washing in PBST for three times (30 min for each time) and Alkaline Phosphatase (AP) buffer for twice (5 min for each time), the slides were visualized in AP buffer containing NBT and BCIP (0.8 μL of NBT and 3.0 μL of BCIP in 1 mL) and developed in the dark environment for 2-20 hr.

RNAscope

RNAscope Fluorescent Multiplex Assay with *Tacr1* probe was performed to determine the labeling efficiency and specificity of *Tacr1-flpo* mice. Brain sections of *Tacr1-flpo* mice that injected with AAV2/9-EF1α-fDIO-EYFP virus were sectioned at 20 μm with a cryostat (Leica CM 1950), and collected into the DepC-PBS. Floating sections were mounted on the slides, heated at 60°C for 2 hr and kept at −80°C before experiments. Slides were pretreated with hydrogen peroxide at room temperature for 20 min and washed in DepC-ddH_2O for 1 min. Then, slides were transferred to the boiling retrieval regent for 7 min and rinsed once in the DepC-ddH_2O at room temperature. Protease digestion was performed in the 40°C HybEZ oven for 15 min. After washing in the DepC-PBS for 3 min and rinsed in DepC-ddH_2O, slides were treated with ethanol twice (3 min for each time) and air-dried at room temperature. Slides were hybridized with the Pre-warmed *Tacr1* probe in the 40°C HybEZ oven for 2 hr. Signal amplification fluorescent label was TSA-based. Anti-GFP staining was performed after the RNAscope staining to define the $EYFP^+$ neurons.

Imaging and analysis

Images were taken using Nikon E80i fluorescence microscope, Nikon Neurolucida microscope, Olympus VS-120 microscope, Nikon NiE-A1 plus confocal microscope, Olympus FV3000 confocal microscope. Cell counting was carried out manually or automatically using Fiji (NIH). Summary plot of the distribution pattern of spinoparabrachial axons and axon terminals was carried out with Fiji (NIH). Briefly, similar areas of brain sections from 3 mice were chosen and aligned together according to the outline of brain sections. After that, sections were set to 8 bits (value of expression level ranging from 0 to 255) and value of each pixel was averaged and plotted. To plot the distribution pattern of PBN_{SC} neurons, similar areas of brain sections from 3 mice were aligned together, the location of PBN_{SC} neurons was marked manually and the markers of similar areas were merged together. Density of PBN_{SC} neurons was calculated as number of neurons in every 10000 μm^2.

QUANTIFICATION AND STATISTICAL ANALYSIS

Statistical analysis was performed using the Igor Pro (Wavemetrics), Prism 6 (GraphPad Software) and MATLAB. Data were analyzed using unpaired Student's t test, paired Student's t test or two-way ANOVA.